scientific reports



OPEN

Stability and functional consequences of disulfide bond engineering in *Aspergillus flavus* uricase

Mohammad Reza Rahbar¹, Navid Nezafat^{1,2}, Mohammad Hossein Morowvat^{1,2}, Amir Savardashtaki³, Mohammad Bagher Ghoshoon^{1,2}, Mohammad Soroosh Hajizade² & Younes Ghasemi^{1,2}⊠

Disulfide bond engineering is a promising strategy for enhancing the stability and functional lifespan of enzymes in therapeutic and industrial applications. In this study, we applied computational modeling to introduce interchain disulfide bonds in Aspergillus flavus uricase to increase its stability without compromising catalytic efficiency. Six uricase muteins were engineered with targeted disulfide bonds at positions selected based on energetic frustration, structural integrity, and tunnel profiling analyses. By employing frustration density mapping, Root Mean Square Fluctuation (RMSF) profiling, and tunnel analysis, we evaluated the structural stability, flexibility, and substrate accessibility of each variant. Our findings revealed that muteins with disulfide bonds between residues such as Ala6-Cys290 and Ser119-Cys220 exhibited significant reductions in highly frustrated regions, enhancing the enzyme's structural resilience. RMSF analysis indicated decreased local flexibility near disulfide sites, contributing to increased stability. Tunnel profiling further demonstrated that muteins with strategically placed disulfide bonds maintained favorable substrate access and low-energy barriers, critical for catalytic turnover. These results underscore the potential of targeted disulfide bond engineering for optimizing enzyme stability, offering valuable insights for the development of stable, high-performance biocatalysts suitable for therapeutic and industrial use.

Keywords Disulfide Bond Engineering, Uricase Stability, Energetic Frustration, Protein Folding Dynamics, Enzyme Tunnel Profiling, In Silico Protein Design

In the rapidly advancing fields of enzyme therapy and industrial biocatalysis, protein stability remains a critical challenge for enhancing catalytic performance and ensuring prolonged functionality under varying conditions. Uricase, also known as urate oxidase (Uox), is a key enzyme in purine metabolism that catalyzes the oxidation of uric acid to allantoin, a soluble compound easily excreted by the kidneys¹. Uricase is naturally found in a variety of organisms, including bacteria, fungi, and many animals, where it helps prevent the accumulation of uric acid—a compound associated with conditions such as gout, hyperuricemia, and kidney disease when present in high concentrations². In humans and other primates, however, uricase is inactive due to evolutionary gene loss, making these populations particularly susceptible to uric acid-related disorders³. Therapeutic uricase enzymes sourced from other species have been explored as treatment options, yet their instability and potential immunogenicity present ongoing challenges⁴.

Structurally, uricase exists as a homotetramer, with each monomer comprising two T-fold domains formed by anti-parallel beta sheets and alpha helices⁵. These subunits associate to create a compact structure with active sites located at the interface between subunits. Notably, each active site is accessed through a narrow tunnel within the tetrameric assembly, which serves as the route for substrate binding and product release. This quaternary structure is both a feature and a limitation, as its compactness contributes to enzyme stability while potentially restricting the active site's accessibility. The structural constraints also make the enzyme vulnerable to

¹Pharmaceutical Sciences Research Center, Shiraz University of Medical Sciences, Shiraz, Iran. ²Department of Pharmaceutical Biotechnology, School of Pharmacy, Shiraz University of Medical Sciences, P.O. Box, Shiraz 71345-1583, Iran. ³Department of Medical Biotechnology, School of Advanced Medical Sciences and Technologies, Shiraz University of Medical Sciences, Shiraz, Iran. [⊠]email: ghasemiy@sums.ac.ir

conformational destabilization under therapeutic conditions, which can further compromise enzyme function and trigger immune responses.

To address these challenges, one strategy is to enhance the stability of uricase through the strategic introduction of disulfide bonds. Disulfide bonds have been shown to act as "molecular staples", linking distant regions of the protein structure and thus reinforcing its overall integrity. They improve resilience by reducing the entropy of the unfolded state, thereby requiring a greater energy input for denaturation. Disulfide bond engineering has been successfully applied in various proteins, leading to enhanced thermal and chemical stability, as demonstrated in uricase from *Aspergillus flavus*. However, while the formation of disulfide bonds can stabilize enzyme structure, it also introduces rigidity that may influence dynamic regions, including tunnels to active sites and catalytic pockets. Disulfide bond placement, particularly within or near active site tunnels, has the potential to impede substrate access and alter the enzyme's catalytic function.

This study seeks to navigate the delicate balance between stability and functionality in uricase by identifying optimal positions for disulfide bond introduction. Through a combination of frustration density mapping, RMSF (Root Mean Square Fluctuation) profiling, and tunnel assessment, we systematically evaluate how these bonds influence uricase's structural integrity and catalytic potential. Frustration density analysis provides insights into regions of the enzyme that are prone to destabilization, which may benefit from the stabilization afforded by disulfide bonds. Tunnel profiling enables us to examine the impact of these bonds on substrate access to the active site, while RMSF measurements assess local and global flexibility, providing a holistic view of how structural modifications affect the enzyme's dynamic behavior.

Recent advances in in silico techniques are significantly transforming enzyme engineering by enabling the design of enzyme variants with enhanced properties. These techniques, which have revolutionized the ability to design new therapeutic options, include molecular dynamics (MD) simulations, protein–protein docking, high-throughput epitope mapping, and machine learning-based design algorithms. MD simulations provide critical insights into enzyme flexibility and stability, aiding the design of more robust and efficient enzyme variants, and also providing information about the dynamics of enzyme active sites. Protein–protein docking helps in understanding enzyme interactions with their substrates or inhibitors, allowing for the design of enzymes with improved specificity and reduced off-target effects¹⁰. High-throughput epitope mapping facilitates the rapid screening of large libraries of enzyme variants, thereby accelerating the identification of promising therapeutic candidates¹¹. Furthermore, machine learning algorithms, particularly those employing deep learning and reinforcement learning, have revolutionized protein structure prediction and enzyme design by enabling the rational selection of key residues responsible for catalytic activity and stability¹⁰. While these in silico techniques offer significant advantages in enzyme engineering, challenges remain in bridging the gap between computational predictions and experimental validation. Additionally, ethical considerations related to AI-driven protein design must be addressed to ensure responsible and transparent use of these powerful technologies.

Our results reveal that certain uricase muteins, engineered with disulfide bonds, exhibit significant reductions in energetic frustration, improved tunnel profiles, and minimized RMSF values, which collectively enhance stability while preserving catalytic accessibility. This integration of structural and functional analyses advances our understanding of enzyme stabilization strategies and offers a blueprint for engineering uricase variants that combine durability with functional efficacy. By doing so, we contribute a novel approach to enzyme engineering, with potential applications across therapeutic and industrial domains.

Through the targeted introduction of disulfide bonds combined with comprehensive computational analysis, this study illuminates pathways for enhancing the stability and function of uricase, providing a comprehensive understanding of disulfide bond engineering in uricase. Our research offers valuable insights for the design of other stable and functional enzymes.

Methods

Data sources

Protein structures used in this study were retrieved from the Protein Data Bank (PDB)¹² at rcsb.org. The uric acid structure obtained from PubChem (https://pubchem.ncbi.nlm.nih.gov/, PID: 1175). Amino acid sequences were obtained from the UniProt Knowledge Base (UniProtKB)¹³ at uniprot.org. The reference structure and sequence for this study were the structure of uricase from *Aspergillus flavus* under UniProt sequence ID Q00511.

Structural analysis

To evaluate the potential impact of mutations on the uricase structure, the mutation sensitivity of each residue was calculated using MaestroWeb¹⁴ (https://www.plus.ac.at/). MaestroWeb is a web interface for the Rosetta protein modeling suite¹⁵.

Disulfide engineering of Aspergillus uricase: Multiple sequence alignment generation

To identify evolutionarily conserved cysteine residues, we performed a multiple sequence alignment (MSA) of the Aspergillus uricase sequence with homologous sequences. Hidden Markov Model (HMM) profiling ¹⁶ within the Yosshi server (<u>Yosshi (msu.ru)</u>) identified structurally similar proteins to Aspergillus uricase in the Protein Data Bank (PDB). The protein with the highest HMM score was selected as a template and aligned with the query sequence using the Smith-Waterman algorithm¹⁷. This initial alignment was iteratively refined based on conserved features observed in the template structure using Musguseal¹⁸ at (<u>Mustguseal: (msu.ru)</u>).

Uricase structure preparation for Yosshi analysis

Uricase, a homotetrameric protein, requires modification for analysis with Yosshi, which requires a singlechain protein structure as input. To address this limitation, we employed the Multiprot.pl standalone software following the developers' instructions as provided by Yosshi server. Multiprot.pl facilitated the processing of the multi-chain uricase structure retrieved from the PDB. The original PDB file contained four separate chains identified by unique chain identifiers. Multiprot.pl modified these identifiers by assigning a single, identical code to all chains. Following chain ID unification, Multiprot.pl renumbered the amino acid residues throughout the entire protein sequence. This process ensured consistent numbering for the newly formed single-chain structure suitable for Yosshi analysis.

Predicting disulfide bonds: Statistical scoring functions in MAESTRO

MAESTRO¹⁴ at https://pbwww.services.came.sbg.ac.at/maestro/web, utilizes statistical scoring functions (SSFs) to analyze the potential formation of disulfide bonds within proteins. These SSFs rely on the analysis of Ca and C β atoms of disulfide-bonded cysteines in a curated dataset of PDB structures. To develop its predictive capabilities, the software was trained on a comprehensive dataset of 1,925 measurements. To develop its predictive capabilities, the software was trained on a comprehensive dataset of 1,925 measurements. This data captured the changes in protein stability observed upon introducing mutations in 55 distinct proteins. This dataset includes structures with high resolution (better than 2.5 Å) and low sequence identity (less than 60%) to ensure diversity and minimize bias.

The core components of MAESTRO's SSFs include the relative frequency of a specific $C\beta$ - $C\beta$ distance observed between bonded cysteines in the reference dataset considered as a penalty (P β). The second penalty, P $\alpha\beta$, evaluates the difference between the C α -C α and C β -C β distances for potential bond partners.

To calculate the final disulfide bond score (Sss), the predicted values for ΔG (free energy change), $P\beta$, and $P\alpha\beta$ are converted to their respective z-scores. These z-scores represent the number of standard deviations a particular value falls from the mean in the reference dataset. Finally, potential binding partners are ranked based on their Sss, with higher scores indicating a greater likelihood of forming a disulfide bond.

Predicting disulfide bond geometry and proximity

Disulfide by Design 2 (DbD2) software⁷, provided by Disulfide by Design (http://cptweb.cpt.wayne.edu/DbD/), was employed to assess residue pairs within the uricase structure. DbD2 analyzes the geometric and spatial proximity of these pairs to determine their suitability for disulfide bond formation. This analysis assumes that if the residues were mutated to cysteines, their positions would allow for proper bond formation based on favorable angles and energetics.

Energetic evaluation using DynaMut2

Prior to introducing mutations, the potential energetic effects of mutation on the reference structure of Aspergillus uricase were assessed using the Dynamut2¹⁹ server as provided at https://biosig.lab.uq.edu.au. DynaMut2 is a computational tool designed to assess the impact of missense mutations on protein stability and flexibility. The algorithm integrates optimized graph-based signatures with normal mode analysis (NMA) to generate consensus predictions. Specifically, DynaMut2 employs two distinct normal mode approaches to analyze and visualize protein dynamics by sampling conformations and evaluating the vibrational entropy changes induced by mutations. This method allows for the estimation of the effects of point mutations on protein stability and flexibility, achieving a high correlation with experimental data (p-value <0.001) and outperforming alternative approaches.

Dynamut2 employs a knowledge-based potential energy function, enabling accurate predictions of the change in free energy ($\Delta\Delta G$) associated with mutations. This computational tool provided valuable insights into the stability implications of candidate mutations.

Mutation and stability analysis using MutationExplorer

Candidate mutations were strategically introduced into the uricase reference structure using MutationExplorer²⁰ at https://mutationexplorer.vda-group.de, a sophisticated computational platform designed for protein stability analysis. MutationExplorer leverages advanced algorithms to calculate the $\Delta\Delta G$ for each mutant, offering a quantitative assessment of the impact on protein stability. Additionally, the platform provides detailed structural visualizations to aid in understanding the potential effects of mutations on protein conformation and interactions.

The fundamental philosophy behind MutationExplorer revolves around the integration of structural bioinformatics and evolutionary principles to elucidate the functional impact of mutations.

Each amino acid substitution in the uricase muteins was analyzed using the MutationExplorer framework. MutationExplorer employs various algorithms to predict the stability changes associated with each mutation, allowing for a comparison between the wild type and muteins.

The outputs from MutationExplorer include stability scores, structural models, and interaction maps, which were further analyzed and interpreted in conjunction with the results obtained from other computational tools used in our study.

Introducing the mutations

Based on a comprehensive analysis of energetic properties, mutation sensitivity, geometric constraints, and evolutionary conservation, four pairs of residues were selected for cysteine substitution. In total, seven mutations were introduced, with one native cysteine residue already present in the wild-type protein (Cys290). A total of six engineered muteins (MUTEIN-1–SMUTEIN-6) were designed. Computational analyses were performed to evaluate their suitability and potential impact on the Aspergillus uricase structure. The mutated sequences were subjected to structure building. The quaternary structure of new sequences with mutated residues to Cysteine were submitted to Multifold²¹ server at https://www.reading.ac.uk/bioinf/MultiFOLD/MultiFOLD_form.htm l. The predicted structures refined by ReFOLD refinement method²² and the AlphaFold2 recycling process. The server additionally assessed the quality of the predicted structures, the most satisfactory coordinates were

selected for further analyses. To insure the achievement of the best relaxed structures, mutated rotamers were refined by rotamer function of UCSF Chimera 1.18, using Dunbrack (2010) rotamer library²³.

Post mutation analyses

Frustration analysis

Uricase is composed of four identical protein chains (a homotetramer), and our engineered mutations were designed to introduce disulfide bonds between adjacent chains, in order to increase its stability. To understand how these modifications could affect the stability of the protein, we used a method called "frustration analysis." This analysis helped us to understand how the mutations that we have introduced may change the balance of stabilizing and destabilizing forces that maintain the protein shape. We used a tool called Frustratometer (available at http://frustratometer.qb.fcen.uba.ar/) to analyze the 3D structure of our wild-type uricase and its six engineered variants. The data were derived from the same structural models obtained in the previous steps of this study. This tool calculates the level of frustration (or structural stress) for each part of the protein structure. These analyses tell us whether the local interactions between residues of the protein are acting to stabilize, destabilize, or if they are neutral. A"highly frustrated" residue experiences a significant degree of destabilization, a"neutrally frustrated" residue has a balance of stabilizing and destabilizing forces, and a"minimally frustrated" residue experiences strong stabilizing forces.

We organized our results into columns representing the residue number and how much frustration it experienced (highly, neutrally, or minimally frustrated). The results were presented as density data, showing how much frustration is present in different parts of the protein. We then compared each mutated variant to the wild-type to see how the engineered disulfide bonds affected these values. To do this we used python and the Pandas library. This method helped us to identify the areas where our mutations had changed the frustration profiles. In order to be more concise, we have only included the relevant results of our analysis in the main body of this paper, and a more detailed description of these results is available in supplementary materials.

Statistical analysis

To determine the statistical significance of the frustration density differences between the wild type and each mutein, a two-sample t-test was applied. For each mutein, average differences in highly frustrated, neutrally frustrated, and minimally frustrated densities were calculated compared to the wild type. A two-tailed t-test was performed for each frustration category to assess whether the differences were statistically significant at a 95% confidence level (p-value < 0.05).

Root mean square fluctuation (RMSF) analysis

RMSF analysis was performed to evaluate the changes in residue flexibility introduced by mutations designed to form disulfide bonds in uricase muteins. The RMSF values of the wild-type uricase (WT) and six muteins (MUTEIN-1–SMUTEIN-6) were calculated using the CABsFlex²⁵ web tool provided at https://biocomp.chem.uw.edu.pl/, which estimates protein flexibility based on coarse-grained molecular dynamics simulations. Each residue's fluctuation was computed for all four chains of the uricase enzyme (chains A, B, C, and D).

The RMSF values were analyzed over the residue range 1 to 301 for each chain, with each chain's results aggregated to evaluate the overall flexibility change.

To evaluate the dynamics of the two protein structures, which includes the wild-type and mutein homote-tramer, two sets of molecular dynamics (MD) simulation was performed. The topology files were generated using the AMBER99SB-ILDN force field. The system was solvated with the SPC216 water model, and an electrolyte concentration of 0.15 M NaCl was added to replicate physiological conditions. The simulations were conducted using GROMACS version 2024²⁶. The system was placed in a cubic box under periodic boundary conditions, ensuring a minimum distance of 1.0 nm between the protein and the box walls. The LINCS algorithm was used to constrain all covalent bonds involving hydrogen atoms. NVT and NPT ensembles were generated and equilibrated at 300 K and 1 bar, using the V-rescale thermostat and Parrinello-Rahman barostat, respectively. Prior to the production run, energy minimization was performed using the steepest descent algorithm. The MD simulation was run for 100 ns for each set, and subsequent analyses were conducted on the resulting trajectories.

To assess the stability and flexibility of the complex, several analyses were performed, including root-mean-square deviation (RMSD) and root-mean-square fluctuation (RMSF). The Gromos clustering algorithm²⁷ was applied to the trajectory to reduce the large number of frames into a representative set, with clusters identified based on a cutoff of 0.15 nm. The structure with the largest number of neighbors was selected and removed from further clustering. Data visualization and plot generation were conducted using QtGrace and Microsoft Excel 2019.

Statistical analysis

To quantify the effect of mutations on flexibility, the following steps were taken

The mean RMSF values for all residues (Global RMSF Comparison) were calculated for both the wild type and each mutein. A paired t-test was used to compare the global RMSF between each mutein and the wild type, determining whether the mutations led to significant changes in overall protein flexibility.

For mutation-specific residues (Local RMSF Comparison), the RMSF values were compared between the wild type and muteins. The analysis focused on residues where mutations were introduced to determine if local flexibility was significantly affected. For each mutation site, the RMSF values across all chains were averaged and compared using a paired t-test at a 95% confidence level (p-value < 0.05). P-values were calculated to assess the

statistical significance of the differences between the wild type and muteins, with results considered statistically significant if the p-value was less than 0.05.

Tunnel detection and energetic barriers of substrate to the active site

To understand how substrates might access the active site of uricase, and to determine whether the engineered mutations altered these access pathways, we used a tool called CaverWeb (available at https://loschmidt.chemi.muni.cz)²⁸. This tool allows us to identify and analyze tunnels within proteins, and it is very useful to predict the pathways that molecules may use to access specific regions of the protein. We analyzed the 3D structures of the wild-type uricase and six engineered variants. Before using CaverWeb, we removed water molecules and any other molecules that might have been present and performed some minor calculations to prepare the structure for analysis.

For each structure, we used a probe radius of 1.0 Å to simulate the size of the uric acid molecule, ensuring that we were assessing the right pathways for our substrate. We defined the starting point for all our tunnel searches at the location of the catalytic residues in the active site of uricase, which are already known. We used default parameters to calculate the tunnel pathways, their surfaces, and their characteristics.

The resulting tunnels were evaluated based on their length, their curvature, their narrowest part (bottleneck radius), and the energy that is needed for a molecule to pass through (energetic barriers). By using this method, we could assess how the structural modifications introduced by the engineered mutations impacted these properties and how that could affect the enzyme's function. We compared the results of our engineered variants with the results that we obtained for the wild-type enzyme. The energetic barriers, which were calculated by CaverWeb, provided an estimate of the energy needed for the substrate (uric acid) to travel through the identified tunnels.

To identify the active site, we used the coordinates of known catalytic residues (Lysine 11, Threonine 58, and Histidine 257, Uniprot charged relay system²²) and a probe radius of 1.4 Å was chosen to approximate the size of the substrate uric acid. We used a clustering threshold of 3.5 Å to group tunnels with similar pathways, as this was a setting that ensured we did not repeat analysis of very similar paths. The default values were used for calculations that are not described in detail in this description, as they were not essential for the understanding of the main process. The most favorable tunnel for each protein (that with the best energetic and geometric parameters) was used for our comparative analysis.

We then used CaverWeb to calculate the potential energy barriers along these tunnels, and compared the calculated energies with the geometric parameters of the tunnels, to investigate the effect of the introduced disulfide bonds. Any significant changes in these values were noted and analyzed. The most favorable tunnel for each protein, based on energetic and geometric parameters, was used for analysis, and results were compared to the results obtained with the wild-type.

Contact analysis using Arpeggio

To evaluate the inter-residue contacts and compare the effects of disulfide bond engineering on wild-type uricase and its muteins, we used Arpeggio (https://biosig.lab.uq.edu.au/arpeggioweb/), an online server for calculating interatomic interactions within protein structures²⁹.

Default parameters were used to define the interaction types. The server calculates the following types of interactions:

Van der Waals (VdW) interactions, Hydrogen bonds (H-bonds), Covalent bonds and clashes, Ionic interactions, Hydrophobic contacts, Aromatic interactions, Polar and water-mediated contacts. The default interaction cut-offs provided by Arpeggio were applied, including: Van der Waals interactions within 4.0 Å; Hydrogen bonds with donor-acceptor distances of 3.0 Å or less; Ionic interactions defined by proximity of charged residues; Hydrophobic contacts between non-polar side chains within 5.0 Å.

For each variant (wild-type and muteins), the total number of inter-residue contacts was calculated, as well as a breakdown of each interaction type. Specific attention was given to residues involved in stabilizing the tetrameric structure of uricase and any potential disruptions caused by disulfide bond introduction.

A comparative analysis of the total contacts between wild-type uricase and the muteins was performed, focusing on changes in: the number of Van der Waals and hydrogen bond interactions. The presence or absence of covalent interactions. Polar and aromatic contacts that could influence the structural stability and substrate binding.

Differences in the total number of contacts, as well as specific interaction types (e.g., hydrogen bonds and Van der Waals forces), were statistically analyzed to determine the significance of any observed changes between wild-type and mutein structures. Changes in interactions that could influence the functionality and stability of uricase were carefully assessed and discussed in the context of substrate binding, quaternary structure, and enzymatic activity.

Results

Available uricase structures

A search for 'uricase' at the RCSB Protein Data Bank (PDB) yielded 121 experimentally resolved structures since 2000, reflecting the extensive research on this enzyme. Among these structures, we selected the X-ray diffraction crystal structure of urate oxidase from *Aspergillus flavus* (PDB ID: 4D12) for the present study. This choice was based on several factors such as high resolution (1.4 Å); matching reference sequence (UniProtKB ID: Q00511); suitability for analysis due to its high quality. The structure, designated as 4D12 for simplicity, has been used in several earlier studies and provides a reliable reference for our analysis.

Residue pairs	D(Ca-Ca)*	D (Cβ-Cβ)*	Disulfide occurrence**	Disulfide frequency***
Ala 6—Cys 290	4.14	4.21	4	0.40
Ala 235—E 236	3.80	5.30	1	0.1
Gly 139—Ileu 140	3.78	N/A	1	0.1

Table 1. The evolutionary conserved cysteine pairs. Table shows the actual residues in modern *Aspergillus flavus* urate oxidase. *Distances between two $C\alpha$ and two $C\beta$. **Disulfide occurrence is a positive integer representing the number of times these positions are occupied by cysteines across homolog sequences. ***This value ranges from 0 to 100% and is obtained by dividing DOccur by the total number of proteins included in the multiple sequence alignment.

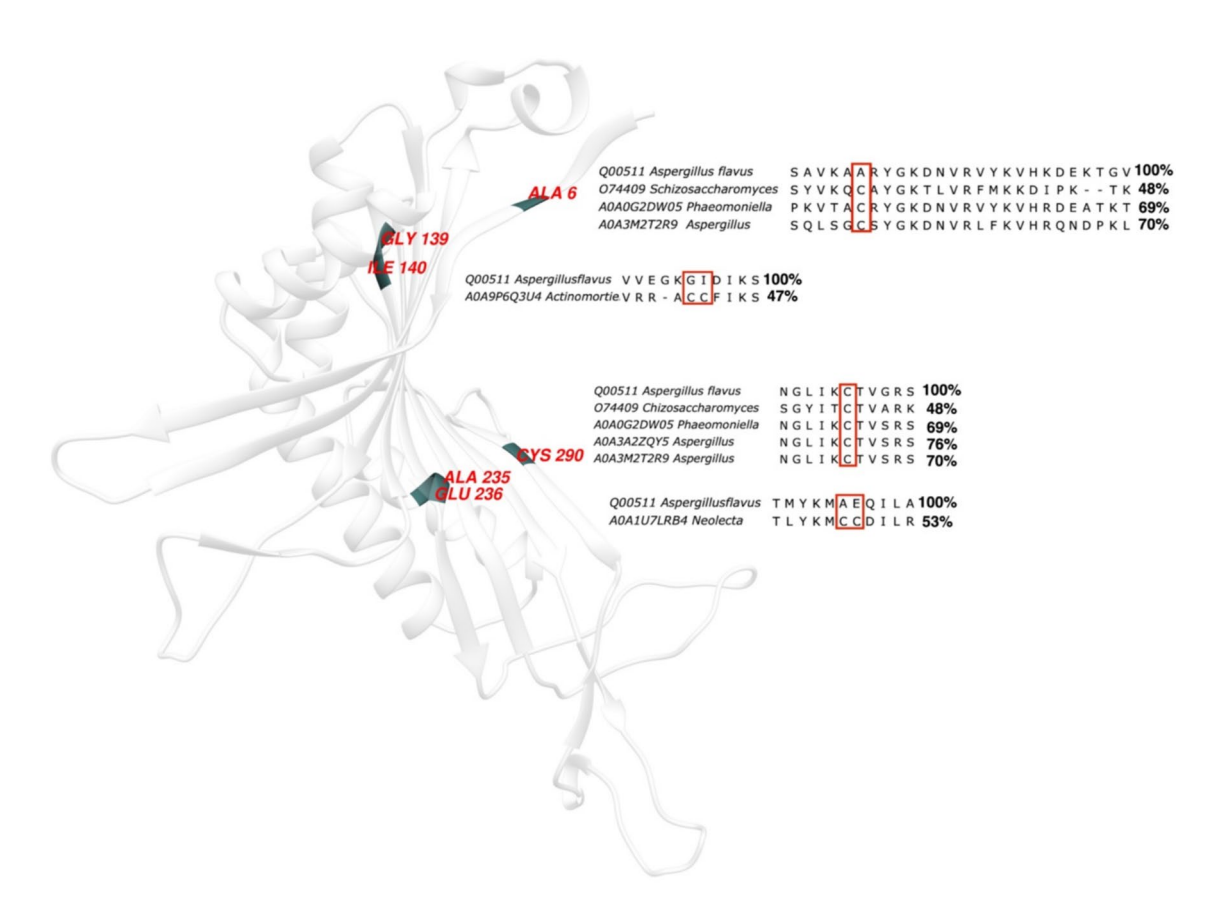


Fig. 1. Predicting Disulfide Bonds and Homolog Conservation. The left panel shows the protein structure with potential disulfide bonds highlighted in green. These green highlighted residues are cysteines, or positions that could be mutated to cysteines, that are close enough in space to form a disulfide bond. The right panel shows an alignment of the query protein sequence to homologous proteins. The homologous proteins all contain cysteines in positions that correspond to the green highlighted residues in the query protein structure. The protein image generated using UCSF Chimera (v1.18); the alignments were generated and visualized by Jalview version: 2.11.4.1³⁰.

Evolutionary conservation of cysteine residues

To identify proper locations for introducing cysteine mutations in Aspergillus uricase, the conservation of cysteine residues across homologous protein sequences from various organisms was analysed. Multiple sequence alignment (MSA) of the uricase family revealed three pairs of residues consistently occupied by cysteines or could be mutated to cysteine (Table 1). While maintaining protein structure and function, this evolutionary conservation suggests that these positions (Fig. 1) might be well-tolerated for cysteine introduction.

Geometric and energetic assessment

Maestro Web

To pinpoint potential disulfide bond formation sites within the protein structure, we employed the Maestroweb tool. This computational approach initiated with a geometric analysis, identifying all cysteine pairs positioned

within a critical 5 angstrom $C\beta$ - $C\beta$ distance threshold. These pairs were considered as potential candidates for disulfide bond formation.

Subsequently, a more refined evaluation was undertaken, integrating geometric considerations with energetic assessments. A combined score, termed Sss, was calculated by considering both the geometric feasibility of bond formation and the associated energetic penalty ($\Delta\Delta G$). By meticulously weighing these factors, the most promising locations for disulfide bond engineering were defined (Table 2).

Disulfide by design 2

An analyze of B-factor of the region of protein to have potential of forming thermo-stabilizing disulfide bonds identified (Table 3). The geometry and energy of the disulfide bond considered in this evaluation.

Sensitivity profile of uricase structure

To predict how specific mutations may alter protein stability, functionality, and interaction networks a profile containing stability changes with confidence for each prediction. This holistic approach facilitates a comprehensive understanding of mutation effects, guiding rational protein design and engineering efforts. The relative mutation sensitivity of candidate residue for mutation to cysteine is depicted in Fig. 2.

The sensitivity profile of each residue in the structure of uricase was assessed (Supporting data 1). Positive $\Delta\Delta G$ (stability Changes) values indicate mutations that are likely to destabilize the protein, suggesting an increase in free energy. Negative $\Delta\Delta G$ values suggest stabilizing mutations, which may decrease free energy and contribute to greater stability. The $\Delta\Delta G$ values vary widely, from as low as -0.804 (A225 W) to as high as 0.527 (A220G). Notably destabilizing mutations include residues like: A6G (0.404), A220G (0.527), D283G (0.473).

Highly stabilizing mutations include: A6 W (-0.693), S119 W (-0.571), and A225 W (-0.804).

High C_pred values (generally \geq 0.85) indicate a greater confidence in the prediction's accuracy. The C_pred values consistently show high confidence across many mutations, with most values clustering around 0.8 to 0.9. D283 K has the highest C_pred value at 0.887, suggesting high confidence for this mutation. Other residues like D283S (0.908) and D283 V (0.896) also have high confidence predictions.

Mutation sensitivity profile demonstrates a wide range of potential mutations, providing insights into the stability effects and confidence levels for each candidate. Residues like S119, A220, and D283 are of particular interest due to their favorable stability profiles and high prediction confidence, making them potential candidates for further experimental validation (Table 4).

Final decision on cysteine introduction

Based on a comprehensive analysis of favorable geometry, energetic states, and evolutionary data for each proposed residue pair, seven positions were selected as potential sites for cysteine mutagenesis to induce disulfide bond formation within the protein. Notably, one position (290) is already occupied by a cysteine residue in the wild-type protein. As planned, each mutant protein could potentially form eight disulfide bonds between four chains. This strategic selection resulted in the generation of six distinct mutants (Table 5).

The average distance and Gibbs free energy

These parameters help in understanding the spatial and energetic consequences of the mutations, and how they may affect the stability of the enzyme.

Table 6 represents the data on average distance, sum of Gibbs stability ($\Delta\Delta$ GStability), and predicted Gibbs stability for each of the muteins of uricase.

Average distance represents the mean distance between specific residues or interacting chains within the uricase homotetramer. Mutein 3 has the largest average distance (57.82), which may suggests a more expanded or less compact structure. This structural extension could reflect significant conformational changes. Mutein 5 has the smallest average distance (14.56), suggesting a more compact structure. This could imply tighter packing of the residues or chains, potentially affecting accessibility or interaction dynamics.

Sum $\Delta\Delta G$ Stability represents the aggregate Gibbs free energy change between the mutant and the wild-type enzyme. Positive values (in this particular analysis, Dynamut2 server) indicate stabilizing mutations, while negative values suggest destabilizing mutations.

Mutein 3 has a positive $\Delta\Delta G$ value of +3.01, which indicates that this mutein is likely more stable than the wild type. This aligns with its larger average distance, as structural expansion in some cases stabilizes the protein by reducing intrachain or interchain strain.

Mutein 1 and Mutein 6 show negative $\Delta\Delta G$ values of -4.54 and -3.67, respectively, indicating destabilizing effects. Despite Mutein 1 having a moderate average distance (42.79), it appears to be destabilized by its structural alterations.

Mutein 5 has a nearly neutral $\Delta\Delta G$ value (-0.24), suggesting it is close in stability to the wild type, with minimal energetic deviation.

The Predicted $\Delta\Delta G$ Stability values provide an additional assessment of thermodynamic stability. Here, positive values indicate stabilizing effects, while negative values suggest potential destabilization.

Mutein 3 and Mutein 4 both show positive $\Delta\Delta G$ predictions (+ 0.96), reinforcing that they may be stabilized compared to the wild type. This suggests that the mutations in these muteins favorably impact stability, which could be due to structural rearrangements that relieve strain or enhance favorable interactions.

Mutein 1, Mutein 2, and Mutein 6 show negative predicted values, with Mutein 2 (-1.7) being the most destabilized. This aligns with their sum $\Delta\Delta G$ values, indicating destabilization.

Mutein 5 has a slightly negative prediction (-1.16), indicating a minor destabilization relative to the wild type, consistent with its compact structure.

Topmutants		ΔΔG pred*	c_pred**	S_ss***
K90	Y91	1.137	0.717	2.719
Y8	I288	1.556	0.728	2.245
V73	F79	1.276	0.670	2.242
F120	L152	1.274	0.704	2.240
Y16	E31	0.522	0.739	1.794
K17	Y30	0.801	0.487	1.696
V15	M32	0.798	0.782	1.693
M231	Y250	2.358	0.653	1.563
V29	W106	1.770	0.733	1.521
K23	T24	-0.199	0.672	1.512
W160	G161	-0.032	0.691	1.475
L252	I288	0.415	0.767	1.463
G139	I140	-0.328	0.681	1.394
D283	P284	-0.233	0.702	1.337
E126	L149	0.260	0.664	1.323
A220	E221	-0.446	0.679	1.288
G193	L194	-0.459	0.665	1.276
P117	H118	-0.259	0.654	1.269
K4	A5	-0.470	0.632	1.266
E246	T247	-0.499	0.670	1.240
T47	K48	-0.292	0.636	1.239
S299	K300	-0.295	0.726	1.236
F191	V197	0.869	0.618	1.207
T155	N156	-0.335	0.659	1.200
D21	V26	0.240	0.723	1.188
S282	D283	-0.419	0.680	1.125
T271	G272	-0.450	0.664	1.096
G272	K273	-0.467	0.663	1.081
T150	D181	-0.586	0.649	1.063
V26	P117	-0.303	0.683	1.047
Y16	F278	1.338	0.808	1.032
I142	W188	1.256	0.801	1.030
G40	E41	-0.524	0.641	1.029
R7	E39	-0.389	0.541	1.012
S147	G148	-0.549	0.640	1.007
N12	P284	-0.399	0.672	1.003
Y46	Q228	0.231	0.706	0.979
I238	V248	0.481	0.764	0.967
I42	V53	0.220	0.728	0.963
T63	Y167	0.598	0.668	0.961
A225	S226	-0.616	0.610	0.946
W186	I245	1.058	0.786	0.933
S192	G193	-0.651	0.595	0.914
I140	F191	1.160	0.699	0.871
N51	I54	-0.260	0.694	0.853
E126	G148	-0.535	0.656	0.838

Table 2. Maestroweb candidates for disulfide engineering. * $\Delta\Delta G$ _pred: Predicted change in free energy ($\Delta\Delta G$), similar to DynaMut2. **c_pred: This could be a prediction related to the compactness or folding energy of the mutant protein. MaestroWeb's c_pred value, ranging from 0 to 1, estimates the confidence in the predicted $\Delta\Delta G$ value, with higher values indicating greater confidence. ***S_ss: A specific score or parameter related to the stability or structural changes introduced by the mutation.

Mutein 3 emerges as a potentially more stable mutant based on both positive $\Delta\Delta G$ values and the expanded average distance, indicating structural changes that may relieve strain or enhance interactions, contributing to stability.

Mutein 4 also shows stability enhancement through positive predicted $\Delta\Delta G$, suggesting its mutations may favorably impact thermodynamics, although it has a moderate average distance.

Muteins 1, 2, and 6 exhibit negative $\Delta\Delta G$ values, indicating destabilizing effects. Mutein 1 and Mutein 6 particularly stand out as more destabilized due to significant negative $\Delta\Delta G$ values.

Mutein 5, with the shortest average distance and near-neutral stability metrics, appears relatively similar to the wild type but with minor destabilizing tendencies.

Tertiary structure building

The requirement of preceding steps was the reference structure of the *Aspergillus flavus* uricase, the available crystal structure under accession number 4D12. After strategically selecting the mutations, new sequences required a reliable quaternary structure. To predict the structural consequences of the introduced mutations, multiple conformations for each mutant were generated using the Multifold server. Among these generated structures, the model exhibiting the highest quality and consistency with structural and energetic criteria was selected. To further refine the predicted structures, the rotamers of mutated residues were optimized to adopt the most probable conformations. Subsequently, the structures were subjected to energy minimization to alleviate steric clashes and optimize atomic coordinates.

Pocket around the substrate, a comparison

Catalytic pockets of the muteins were assessed to evaluate the detailed interactions an amino acid composition, the values compared to those of wild type. Figure 3, represents the catalytic pocket of wild type uricase and uric acid substrate enclosed in the pocket. MUTEIN-3 has a volume (303.104 ų) and surface area (413.211 Ų) comparable to or slightly better than other muteins, suggesting good potential for binding (Table 7). Enclosure is slightly lower in the wild type, indicating better encapsulation in muteins, especially MUTEIN-4 (0.955). The number of hydrogen bond donors and acceptors, as the functional groups is similar across muteins. MUTEIN-1 shows the highest hydrophobicity ratio (0.707), which might influence its binding capabilities. The ratio of polar amino acids in MUTEIN-3 is notable since it may enhance interaction with aqueous environments or polar substrates. MUTEIN-3 has the same number of polar amino acids as MUTEIN-2 and MUTEIN-5, while the wild type has fewer (8.000).

Based on the comparison MUTEIN-3 stands out with a balanced volume and surface area, along with a favorable hydrophobicity ratio and a good number of hydrogen bond donors and acceptors. It also shows a solid balance of polar and apolar residues, which suggests potential for effective interactions with ligands.

Frustration analysis

To assess the impact of specific mutations on the structural stability of uricase, a frustration analysis was conducted. This analysis evaluates the distribution of frustrated interactions within the protein, categorizing regions based on their frustration levels as highly frustrated, neutrally frustrated, or minimally frustrated (Fig. 4). By comparing these frustration densities between the wild type and each mutein, we can identify shifts in structural stability resulting from the introduced disulfide bonds. Additionally Fig. 5 represent the structures of wild type enzyme and six muteins including the frustration interactions represents by dashes. MUTEIN-2, MUTEIN-3, MUTEIN-4, MUTEIN-5, and MUTEIN-6 show highly significant differences in the highly frustrated density category, while MUTEIN-1 also shows significance in neutral and minimally frustrated categories. MUTEIN-3 shows the most considerable negative difference in both highly and neutrally frustrated densities, indicating that it may be the most stable mutein (Table 8). The p-values for MUTEIN-2, MUTEIN-3, and MUTEIN-4 suggest that these muteins exhibit statistically significant reductions in frustration densities compared to the wild type, particularly in highly frustrated density.

RMSF analysis

The global RMSF comparison shows that muteins MUTEIN-1 and MUTEIN-2 had the largest reductions in flexibility, suggesting enhanced stability.

Local RMSF differences at mutation sites indicate significant changes in flexibility, particularly at residues 6, 290, and 283. Muteins MUTEIN-1 and MUTEIN-2 showed the most pronounced stabilization at mutation sites, while MUTEIN-6 had less significant changes (Fig. 6).

Mutein MUTEIN-3, despite showing the best energy-based stability in the frustration analysis, demonstrates a more complex result in terms of RMSF (flexibility) compared to the wild type. Based on the local RMSF analysis, it appears to have a significant reduction in flexibility (negative local RMSF difference: -0.79) at its mutation sites, which could contribute to its overall stability. However, flexibility and frustration density measure different aspects of protein behavior, so it's possible for a mutein to be highly stable (low frustration) but still show substantial reductions in flexibility (high RMSF change).

MUTEIN-3 exhibits a global reduction in flexibility with a difference of -0.17, indicating that overall, this mutein is less flexible than the wild type. MUTEIN-3 has a substantial negative local RMSF difference of -0.79, which means the mutation sites are much less flexible than their corresponding residues in the wild type. This reduction in local flexibility could be a factor contributing to its stability, especially in the regions that play a critical role in structural integrity. The local flexibility change is moderately significant (p-value =0.148), suggesting that the observed reduction in flexibility at the mutation sites could be biologically relevant.

To evaluate the structural integrity and flexibility of the best mutein (Mutein3), molecular dynamics simulations of wild-type uricase and the cysteine-engineered mutein (Mutein 3: Asn12 Cys, Ala49 Cys, Ala225

Res1 chain	Res1 seq	Res1 AA	Res2 chain	Res2 seq	Res2 AA	Chi3	Energy	Sum B-factors
A	2	ALA	С	295	SER	110.37	0.84	54.36
A	295	SER	С	2	ALA	110.37	0.84	54.36
В	2	ALA	D	295	SER	110.37	0.84	54.36
В	295	SER	D	2	ALA	110.37	0.84	54.36
A	49	ALA	С	225	ALA	-81.79	1.11	14.35
A	225	ALA	С	49	ALA	-81.79	1.11	14.35
В	49	ALA	D	225	ALA	-81.79	1.11	14.35
В	225	ALA	D	49	ALA	-81.79	1.11	14.35
A	283	ASP	С	12	ASN	93.9	1.32	9.7
В	283	ASP	D	12	ASN	93.9	1.32	9.7
A	12	ASN	С	283	ASP	93.9	1.33	9.7
В	12	ASN	D	283	ASP	93.9	1.33	9.7
A	6	ALA	С	290	CYS	119.11	2.34	14.12
A	290	CYS	С	6	ALA	119.11	2.34	14.12
В	6	ALA	D	290	CYS	119.11	2.34	14.12
В	290	CYS	D	6	ALA	119.11	2.34	14.12
A	11	ASP	С	287	LEU	114.51	2.88	9.07
A	287	LEU	С	11	ASP	114.51	2.88	9.07
В	11	ASP	D	287	LEU	114.51	2.88	9.07
В	287	LEU	D	11	ASP	114.51	2.88	9.07
A	14	ARG	D	280	PRO	110.91	3.15	8.92
A	280	PRO	D	14	ARG	110.91	3.15	8.92
В	14	ARG	С	280	PRO	110.91	3.15	8.92
В	280	PRO	С	14	ARG	110.91	3.15	8.92
В	119	SER	С	220	ALA	-86.19	3.29	13
A	119	SER	D	220	ALA	-86.19	3.31	13
A	220	ALA	D	119	SER	-86.19	3.34	13
В	220	ALA	С	119	SER	-86.19	3.37	13
A	170	LEU	С	58	ASP	104.49	3.63	12.19
A	58	ASP	С	170	LEU	104.49	3.64	12.19
В	58	ASP	D	170	LEU	104.49	3.64	12.19
В	170	LEU	D	58	ASP	104.49	3.64	12.19
A	57	THR	С	286	GLY	-103.21	4.08	9.67
A	286	GLY	С	57	THR	-103.21	4.08	9.67
В	57	THR	D	286	GLY	-103.21	4.08	9.67
В	286	GLY	D	57	THR	-103.21	4.08	9.67
A	5	ALA	С	291	THR	95.85		15.07
A	291	THR	С	5	ALA	95.85	4.39	15.07
В	5	ALA	D	291	THR	95.85	4.39	15.07
В	291	THR	D	5	ALA	95.85	4.39	15.07
A	46	TYR	С	232	TYR	-102.3	5.11	12.87
A	232	TYR	С	46	TYR	-102.3	5.11	12.87
В	46	TYR	D	232	TYR	-102.3	5.11	12.87
В	232	TYR	D	46	TYR	-102.3	5.11	12.87
A	161	GLY	С	51	ASN	109.57	6.52	15.23
В	51	ASN	D	161	GLY	109.57	6.52	15.23
A	51	ASN	С	161	GLY	109.57	6.53	15.23
В	161	GLY	D	51	ASN	109.57	6.53	15.23
A	122	ARG	D	150	THR	-92.51	7.78	12.07
В	150	THR	С	122	ARG	-92.51	7.78	12.07
	1 200	11111		122		12.31	/./3	12.07

 Table 3. Energy, angle, B-factor of the mutation candidates.

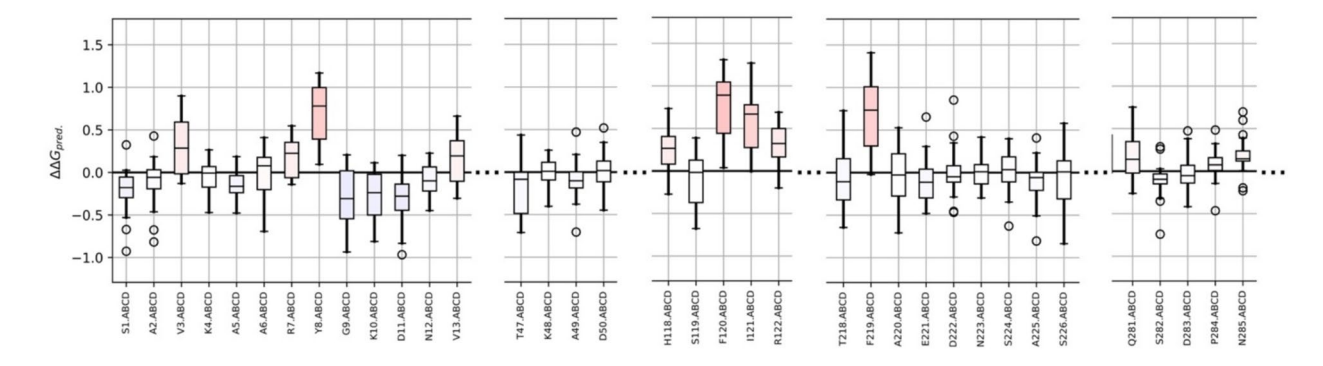


Fig. 2. This figure depicts the relative sensitivity profiles of various uricase mutants compared to the wild-type enzyme. Each bar represents the change in 9868 sensitivity for a specific mutant residue. Blue bars indicate increased sensitivity, while red bars represent decreased sensitivity. The color intensity corresponds to the magnitude of the change.

Residue	ΔΔG	C_pred	Effect on stability	Confidence level
D283 C	-0.052	0.884	Slightly stabilizing	Very high
N12 C	-0.114	0.864	Mildly stabilizing	High
S119 C	-0.202	0.841	Mildly stabilizing	High
A220 C	-0.102	0.839	Slightly stabilizing	High
A49 C	-0.062	0.857	Slightly stabilizing	High
A6 C	0.096	0.842	Destabilizing	High
A225 C	0.005	0.842	Slightly destabilizing	High

Table 4. The top cysteine mutation candidates, highlighting their stability effects and confidence levels.

Mutein	Residue mutation
Mutein 1	Ala6 Cys, Ala220 Cys, Ser119 Cys
Mutein 2	Ala220 Cys, Ser119 Cys, Asp283 Cyst, Asn12 Cys
Mutein 3	Ala49 Cys, Ala225 Cys, Asp283 Cys, Asn12 Cys
Mutein 4	Ala6 Cys, Asp283 Cyst, Asn12 Cys
Mutein 5	Ala6 Cys, Ala49 Cys, Ala225 Cys
Mutein 6	Ala220 Cys, Ser119 Cys, Ala49 Cys, Ala225 Cys

Table 5. The mutation positions for each mutein.

Column1	Average distance	Sum ΔΔGStability	Prediction ΔΔGStability
Mutein 1	42.79	-4.54	-1.07
Mutein 2	31.04	-1.3	-1.7
Mutein 3	57.82	3.01	0.96
Mutein 4	35.4	2.14	0.96
Mutein 5	14.56	-0.24	-1.16
Mutein 6	31.04	-3.67	-1.1

Table 6. The distances energetic states of muteins.

Cys, Asp283 Cys) were performed for 100 ns. RMSD analysis revealed that both structures equilibrated within \sim 10 ns, with the wild-type displaying fluctuations between 0.20–0.40 nm and the mutein displaying slightly lower fluctuations (0.15–0.35 nm) (Fig. 7). The engineered disulfide bonds caused enhanced structural rigidity without compromising the protein's conformational integrity. RMSF analysis demonstrated conserved flexibility patterns across all four chains of both variants, with consistent peaks at residue \sim 25 (0.3–0.4 nm) and the C-terminus (0.8–1.3 nm). The mutein exhibited slightly reduced residual fluctuations in several regions while maintaining the natural dynamic profile essential for catalytic function (Fig. 8).

Tunnel analysis to the active site

To investigate the effects of mutations on substrate access to the active site, a tunnel analysis was performed for each mutein and the wild-type enzyme. The tunnels to the active site and the tunnel profiles are illustrated in Fig. 7. This analysis assesses the binding energy profile along the substrate's pathway from the enzyme surface to the active site, providing insights into potential changes in substrate binding affinity and energy barriers within the tunnel (Fig. 9). By examining variations in these energy profiles, we can infer how mutations may influence the ease or difficulty of substrate passage through the tunnel. Muteins 1, 2, and 6 exhibit lower binding energies compared to the wild-type (-4.2, -5.3, -6.3 vs. -4) (Table 9), indicating potentially stronger substrate binding. Mutein 5, with a drastically different value (13.1), suggests impaired or dysfunctional binding, likely due to significant structural disruptions.

Muteins 1, 2, and 6 show similar trends to E-bound with lower energy barriers, which may imply smoother substrate passage through the tunnel. Mutein 5 again stands out with the same energy (13.1), suggesting a blockage or significant hindrance in substrate flow. The surface energy (E-surface) is relatively consistent across all muteins, showing that the mutations likely don't significantly affect the tunnel's surface energy except for Mutein 5, which is still close to the range, suggesting a moderate impact on substrate entry.

The activation energy remains quite similar among WT and Muteins 1–4. Mutein 6 shows a drop to 0, indicating a potentially more efficient transition from surface to active site. Mutein 5 again deviates significantly

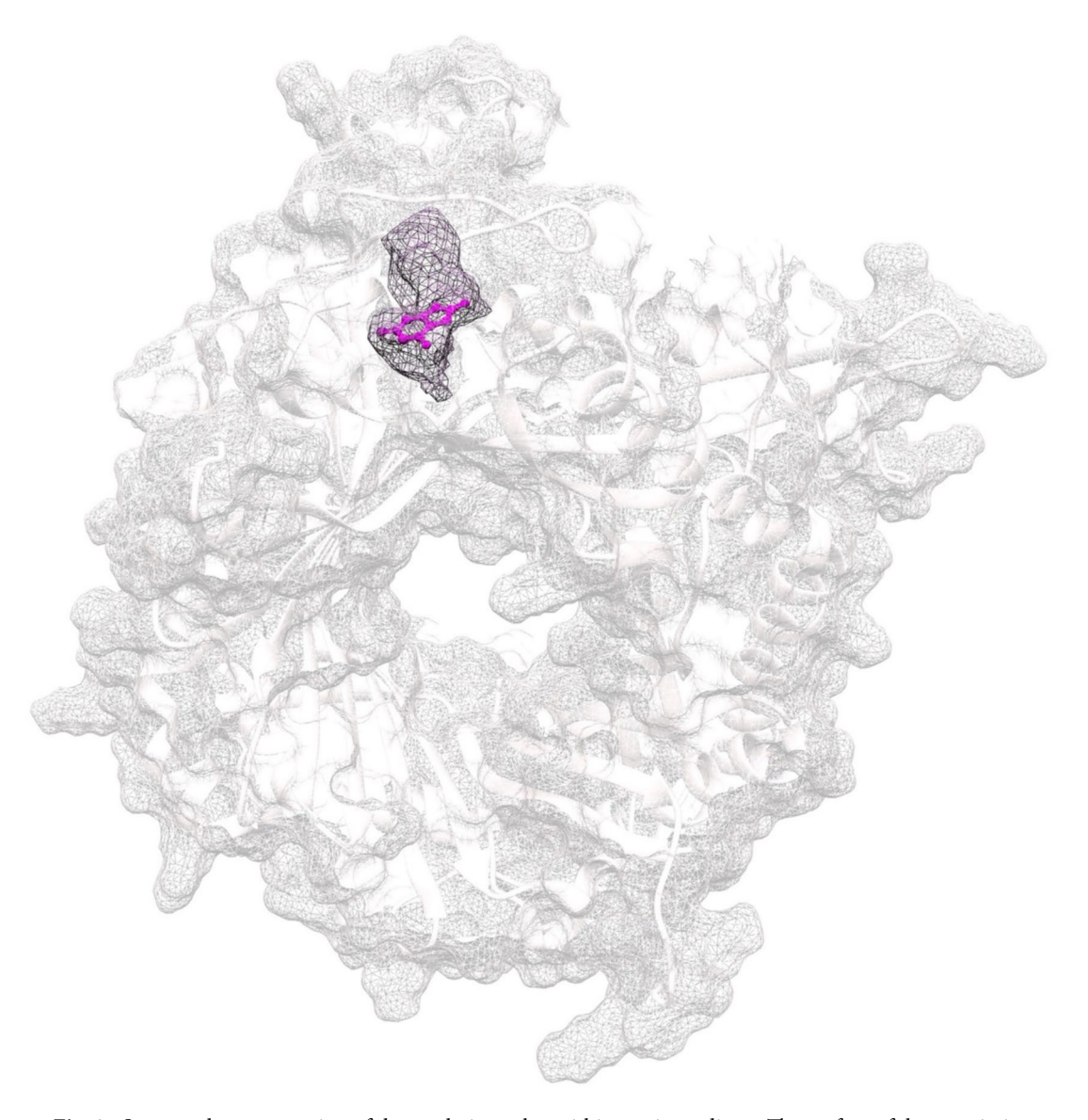


Fig. 3. Structural representation of the catalytic pocket within a uricase dimer. The surface of the protein is displayed as a transparent mesh, providing spatial context, while the backbone is rendered in cartoon ribbons to emphasize secondary structures. The catalytic pocket is highlighted with a mesh overlay, enclosing the uric acid substrate, visualized in purple ball-and-stick format. Image generated using UCSF Chimera (v1.18). The protein models belongs to Aspergilus flavus uricase (PDB ID: 4D12).

Descriptor	Mutein-1	Mutein-2	Mutein-3	Mutein-4	Mutein-5	Mutein-6	WT
Volume [ų]	293.376	301.568	303.104	305.664	298.496	290.304	299.520
Surface [Å ²]	393.967	413.211	413.211	411.622	401.297	400.819	442.963
Depth [Å]	16.159	16.159	16.159	16.159	16.159	16.120	15.430
Enclosure	0.947	0.949	0.949	0.955	0.952	0.948	0.921
Pocket atoms	116	117	117	115	117	111	105
Hydrogen bond donors	12	13	13	12	13	13	13
Hydrogen bond acceptors	10	11	11	11	11	11	11
Hydrophobicity ratio	0.707	0.692	0.692	0.696	0.692	0.694	0.686
Apolar amino acids	11	11	11	11	11	11	11
Polar amino acids	10	11	11	10	11	11	8

Table 7. Pocket characteristic of uricase wild type and muteins.

with a very high value (18), suggesting a severe disruption in tunnel dynamics, impeding the substrate's approach to the active site

 Δ EBS, reflects the energy difference between bound and unbound states, with lower values suggesting more favorable binding. Mutein 6 exhibits the largest reduction (-1.8), meaning it facilitates substrate binding the most. Mutein 5, with a huge positive delta (18), again highlights major issues in substrate binding, likely rendering the enzyme non-functional.

Muteins 1 and 2 show improved substrate binding and lower energy barriers, correlating well with their stabilized structures (based on frustration and RMSF analyses), making them strong candidates for enhanced functionality. Mutein 6 also shows promising results with very low binding energy and a lack of activation energy, indicating potential for increased substrate accessibility (Fig. 9). Mutein 3, despite being the most energetically stable in previous frustration analysis, shows no significant advantage here in terms of substrate binding or tunnel energy dynamics. However, its overall performance remains moderate, and further investigation is needed. Mutein 5 stands out as highly unstable, with severely disrupted energy dynamics. This likely reflects significant structural disruption and a loss of enzyme functionality (Fig. 10).

Total energy calculation

Table 10 shows the total energy of each protein and the differences between these values and that of the wild type. Mutein 3 (-2838.05) and Mutein 5 (-2839.64) have the lowest total energy values, suggesting they are energetically more stable than the wild type. Lower energy generally correlates with higher stability. Mutein 4 also follows closely with a total energy of -2829.17, indicating another relatively stable mutant. Muteins 1 (-2529.49), 2 (-2550.94), and 6 (-2530.17) have significantly higher total energy values compared to Muteins 3, 4, and 5, suggesting that these structures may be less stable.

Total difference to parent

Muteins 3 (-28.3), 5 (-26.71), and 4 (-37.18) have the smallest differences in energy compared to the wild type, reinforcing that their structural changes have a minimal impact on overall stability. These small deviations indicate that the mutations are not significantly disrupting the protein's energy landscape, making them good candidates for improved stability.

Muteins 1 (-336.86), 6 (-336.18), and 2 (-315.41) show much larger differences from the wild type, meaning the mutations in these variants induce substantial changes to the energy profile. This suggests potential destabilization or significant alterations to the overall structure.

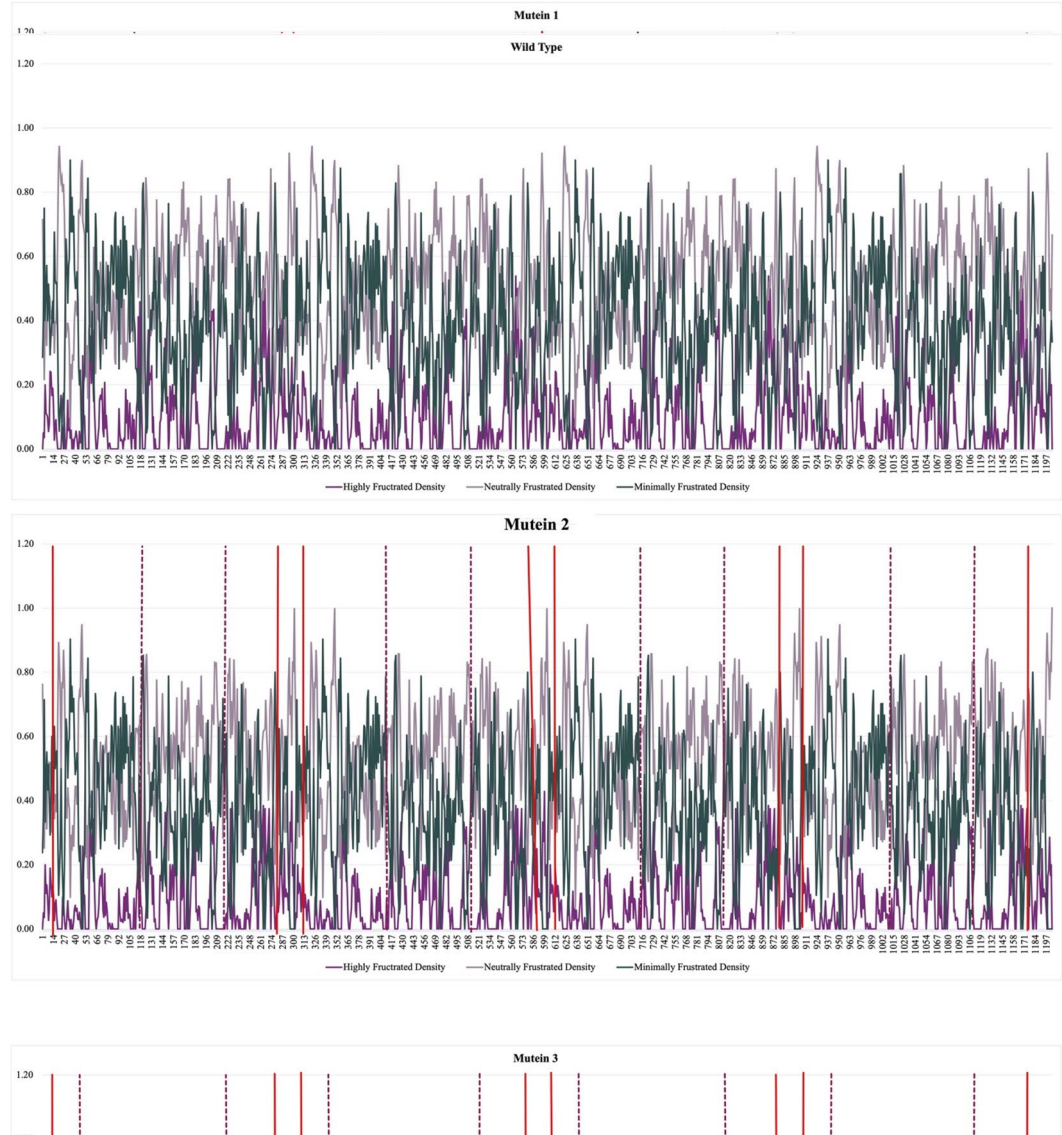
Muteins 3, 5, and 4 demonstrate the best stability based on their lower total energy values and small differences from the wild type. These mutants are likely more structurally stable, and Mutein 3 in particular stands out as having both high energetic and frustration-based stability.

Muteins 1, 6, and 2 show much larger deviations in energy, suggesting they are less stable compared to the wild type, which may compromise their functionality or overall structure.

Protein contacts

The total number of interactions and the breakdown of various types (such as van der Waals, hydrogen bonds, ionic interactions, etc.) provide detailed information about how the mutations affect molecular interactions within the uricase enzyme (Table 11). These interactions could potentially contribute to the stability and functionality of the muteins. Here's how this data might be relevant to your research in the context of stability and mutations:

The number of van der Waals (VdW) interactions decreases significantly in the muteins compared to the wild type, which might indicate a reduction in stabilizing non-covalent interactions. However, this could be balanced by other forms of stabilization, such as hydrophobic contacts. Polar contacts (both direct and weak) are reduced slightly in all muteins, suggesting subtle alterations in electrostatic or hydrogen-bonding interactions that might impact flexibility or stability.



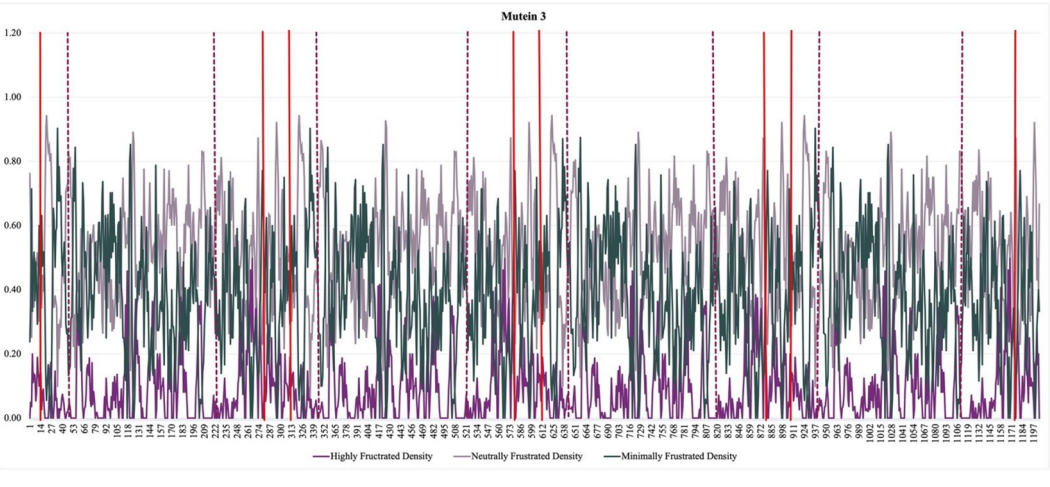
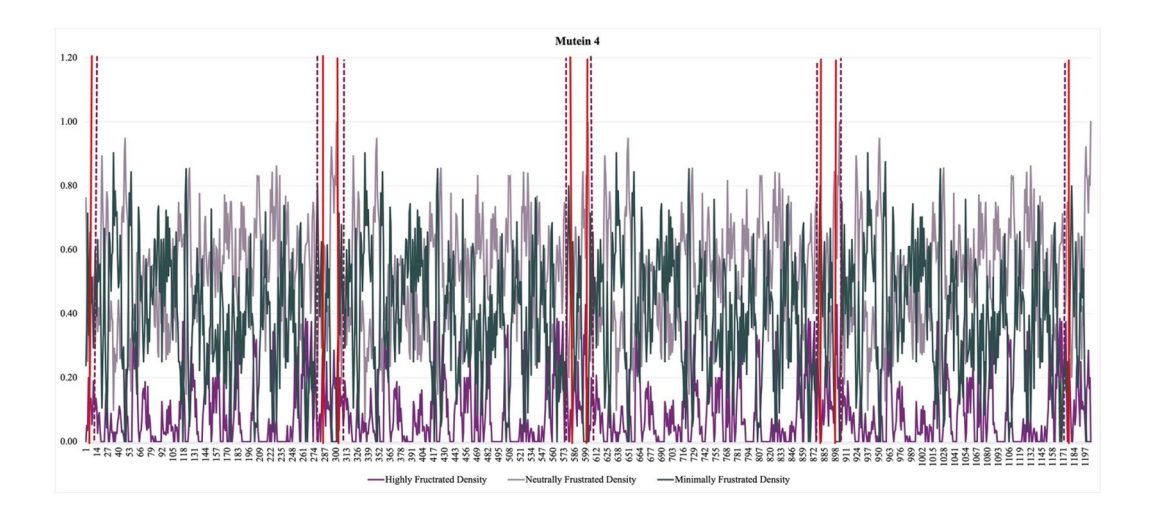
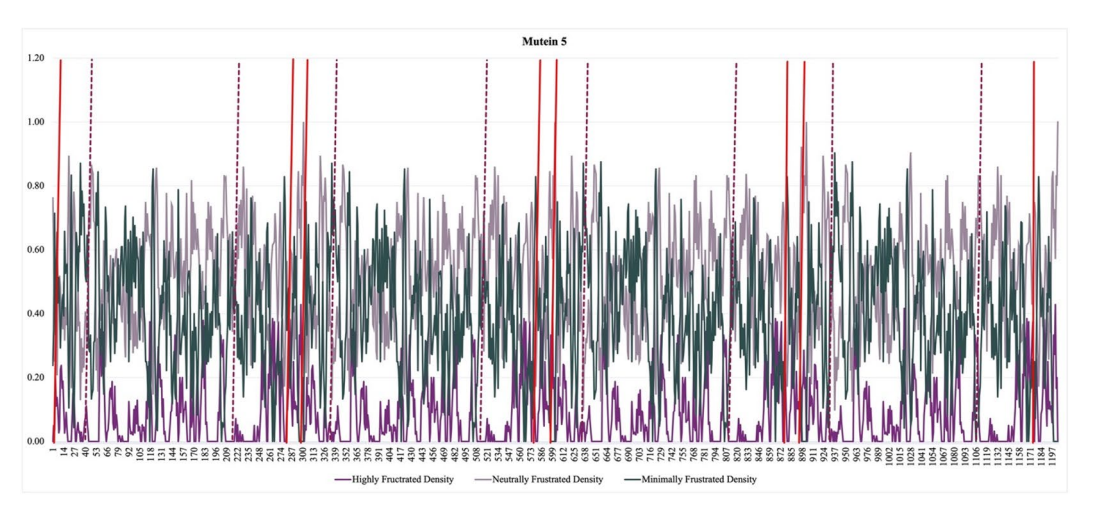


Fig. 4. Residue frustration density analysis. This line graph depicts the frustration density distribution across the protein sequence. The x-axis represents residue numbers, and the y-axis indicates the frustration density. Different colored lines correspond to varying levels of frustration: highly frustrated (red), neutrally frustrated (purple), and minimally frustrated (green). Residue pairs defined by red lines and purple dashes represent potential hotspots for disulfide bond formation.





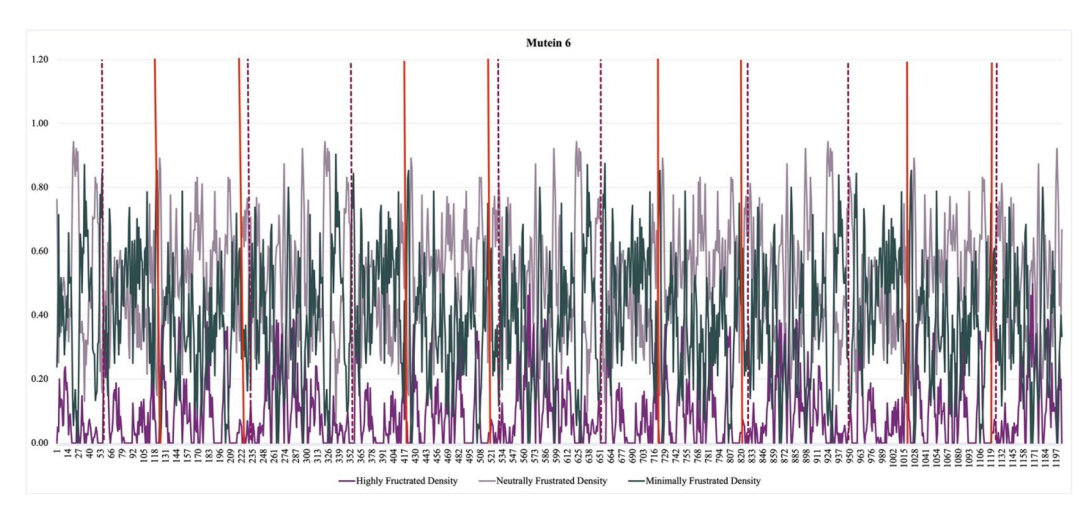


Fig. 4. (continued)

The hydrogen bond count is lower in all muteins compared to the wild type, which might reduce overall stability. However, muteins 1–6 maintain a similar number of hydrogen bonds (around 224–228), suggesting that these bonds remain relatively conserved among the mutants.

Water-mediated hydrogen bonds are absent in the muteins but present in the wild type. This absence may affect how water molecules stabilize the protein, possibly contributing to changes in flexibility or binding efficiency.

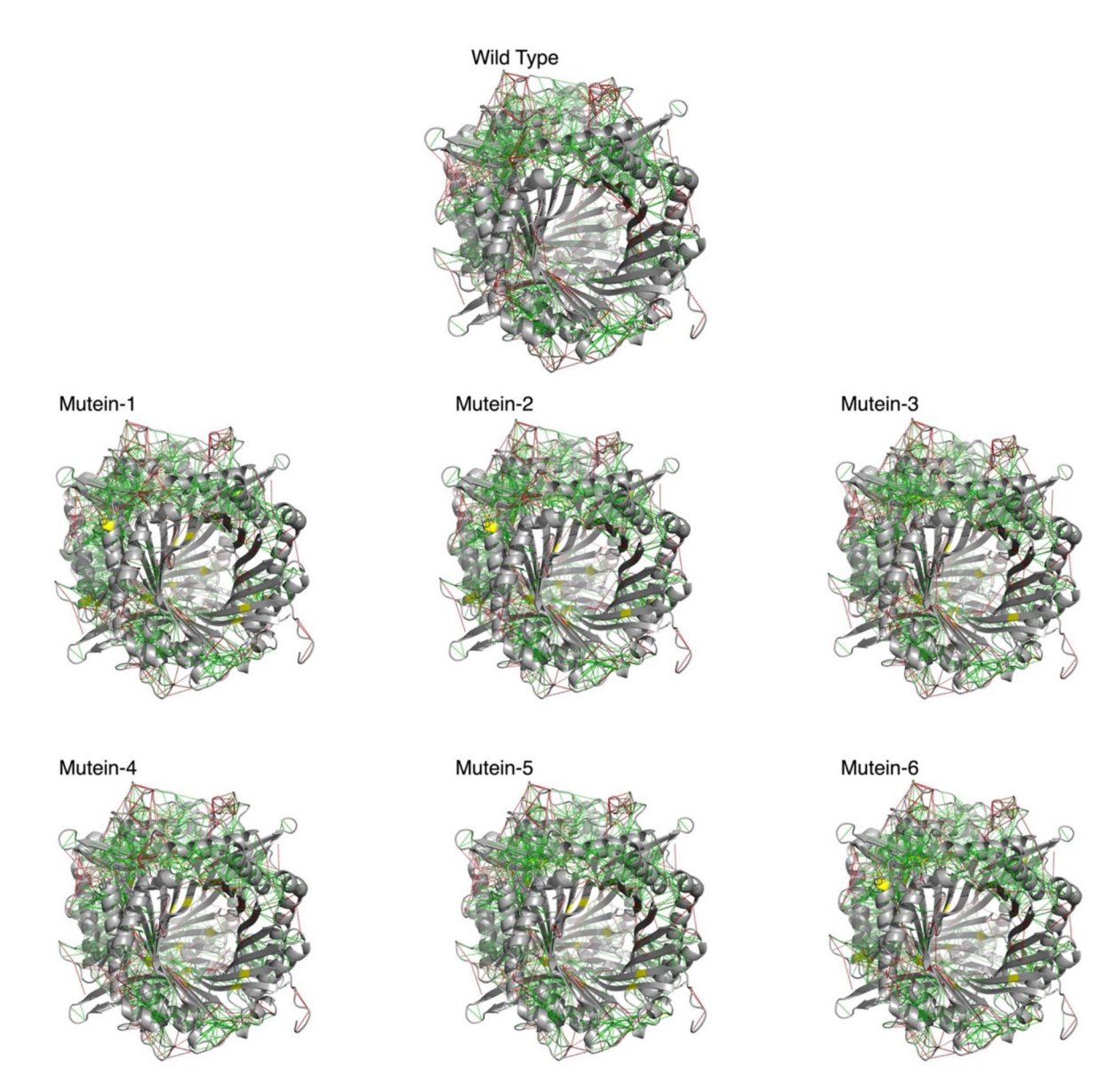


Fig. 5. Frustration density distribution across Uricase structure. This visualization presents the uricase homotetramer in a ribbon cartoon format (gray), with frustration density mapped onto its structure. Highly frustrated interactions are marked by red dashed lines, while minimally frustrated interactions are represented by green dashed lines. Cysteine mutations are highlighted in yellow, indicating positions of potential disulfide bond formation aimed at enhancing structural stability. This structural frustration analysis elucidates the potential stabilization conferred by specific residue mutations. The visualization scripts were generated by frustratometer server at (available at http://frustratometer.qb.fcen.uba.ar/), the script then *visualized using PyMOL version 3.0.0*.

Interestingly, hydrophobic contacts increase in most muteins (except Mutein 6), which might suggest enhanced stability in the hydrophobic core of the protein. Hydrophobic interactions are key to protein folding and stability, so this increase could be stabilizing in the absence of other non-covalent interactions.

Aromatic contacts are also slightly more prevalent in the muteins, which could be a stabilizing factor, though the change is minimal.

Covalent and clash interactions

The reduction or elimination of covalent interactions and clash interactions in the muteins is noteworthy. These clash interactions in the wild type might have caused some destabilization, and their absence in the muteins could lead to a more stable conformation.

The fact that mutually exclusive interactions (non-overlapping interactions) are drastically reduced in muteins compared to the wild type could suggest an overall less crowded or more optimized interaction network, contributing to better flexibility or functional efficiency.

	Highly frustrated difference	p-Value highly frustrated	Neutral frustrated difference	p-Value neutral frustrated	Minimally frustrated difference	p-Value minimally frustrated
Mutein-1	-0.017477	0.051981	-0.12481	1.25E-07	0.142287	2.89E-06
Mutein-2	-0.059387	0.000014	-0.122658	5.57E-06	0.182044	2.01E-06
Mutein-3	-0.17668	0.000008	-0.044691	1.31E-01	0.221371	1.13E-10
Mutein-4	-0.052436	0.000188	-0.059812	2.45E-02	0.112248	1.71E-03
Mutein-5	-0.142688	0.002567	-0.012536	5.85E-01	0.155224	2.18E-05
Mutein-6	-0.14926	0.000303	-0.036766	1.75E-01	0.186026	6.11E-06

Table 8. Frustration differences in comparison to wild type. (A negative value indicates that the mutein has lower highly frustrated density compared to the wild type, suggesting improved stability. Similar interpretation applies for neutrally and minimally frustrated densities); positive values in these columns imply that the mutein maintains or increases stability in those categories compared to the wild type. A p-value less than 0.05 typically suggests that the difference is statistically significant.

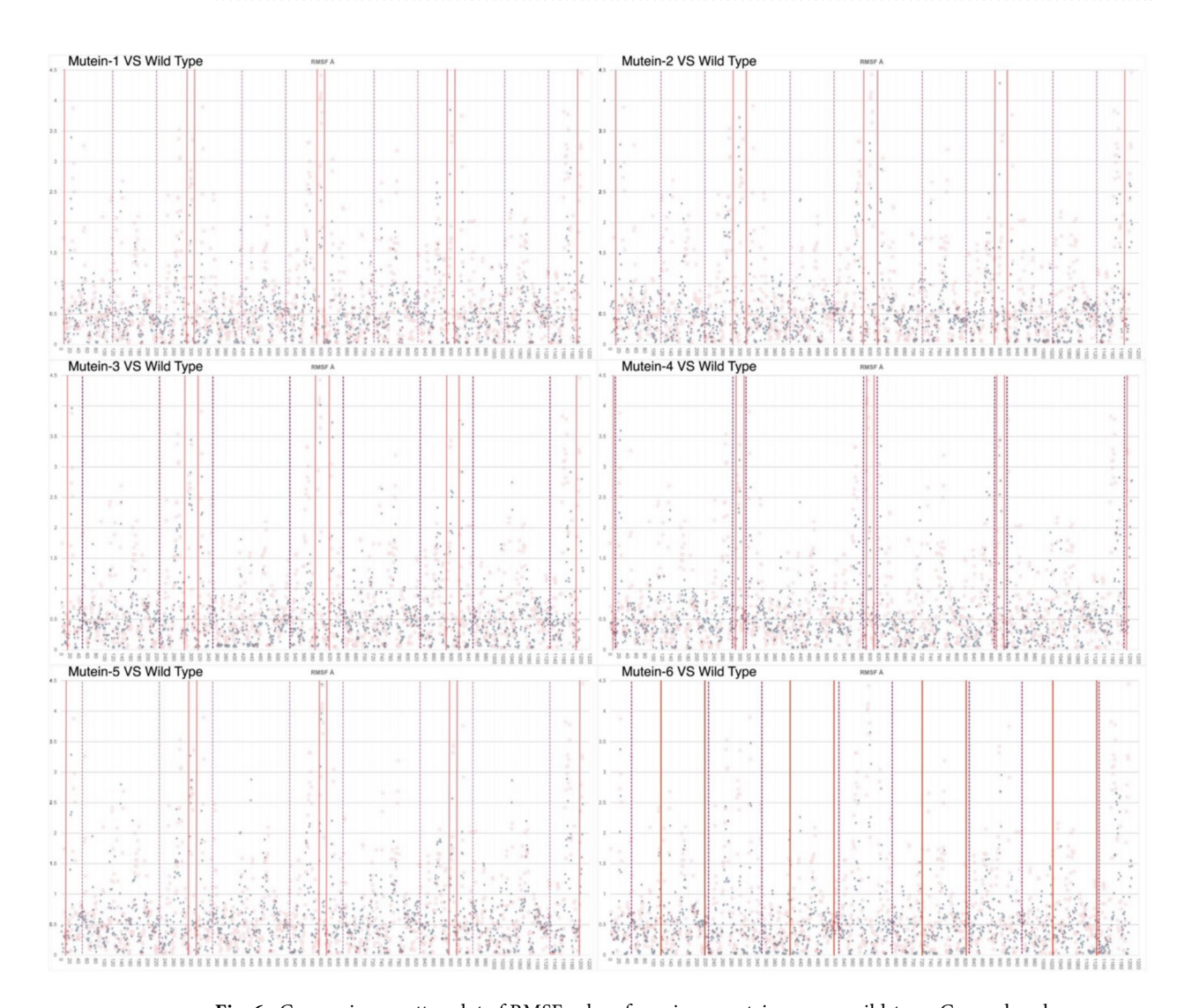


Fig. 6. Comparison scatter plot of RMSF values for uricase muteins versus wild-type. Green rhombuses indicate RMSF values of each residue in the muteins, while corresponding wild-type values are shown as semi-transparent red circles. Hotspot residues mutated to cysteine are marked with red vertical lines and purple dashes. The x-axis denotes residue numbers, while the y-axis represents RMSF values in angstroms, highlighting structural flexibility across the variants.

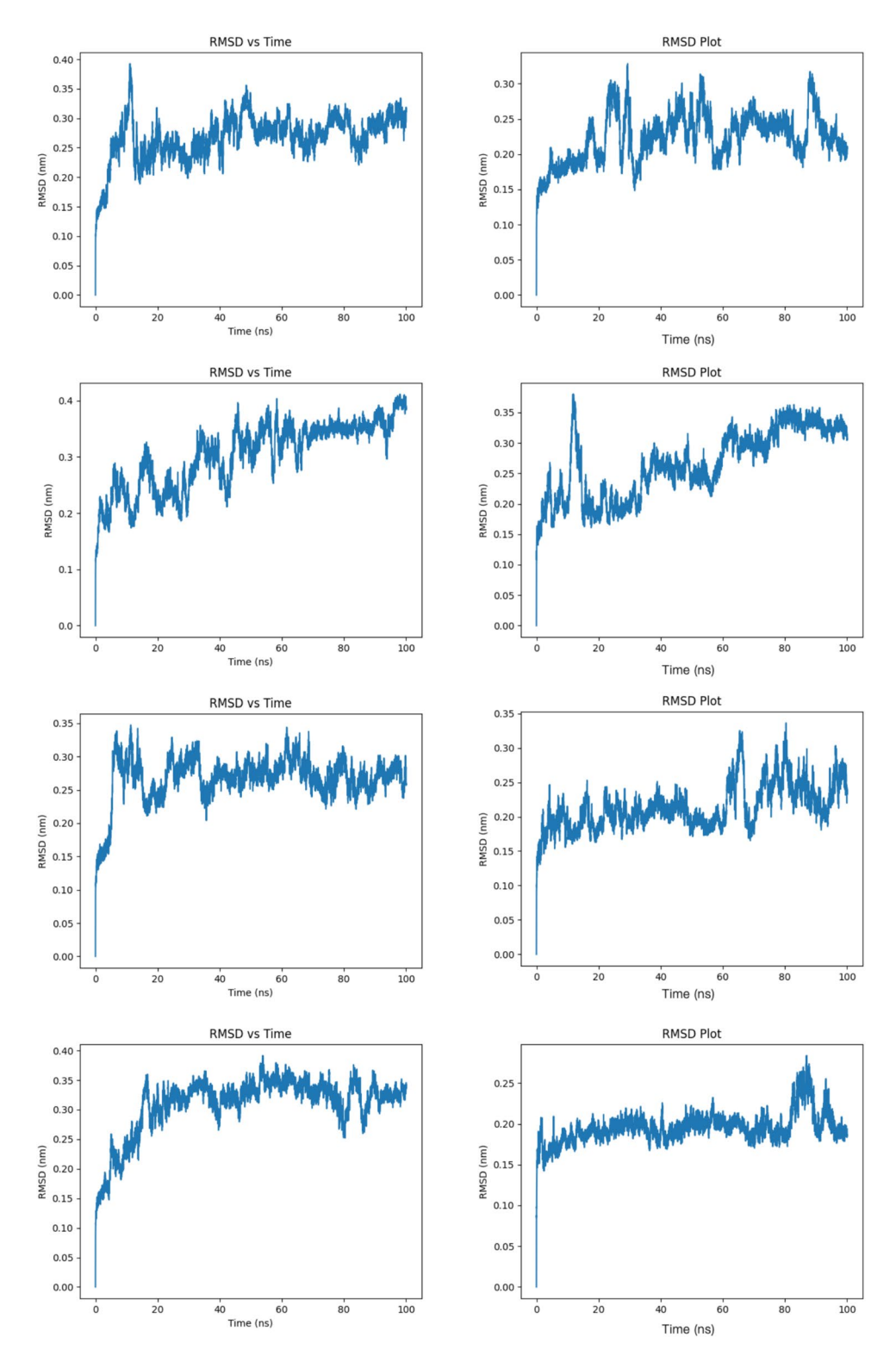


Fig. 7. RMSD analysis of wild-type A. flavus uricase (left panels) and disulfide-engineered mutein (right panels) over 100 ns molecular dynamics simulation. Each row represents one simulation replicate. The mutein (Asn12 Cys, Ala49 Cys, Ala225 Cys, Asp283 Cys) demonstrates slightly reduced conformational fluctuations compared to wild-type, indicating enhanced structural stability conferred by the engineered inter-chain disulfide bonds.

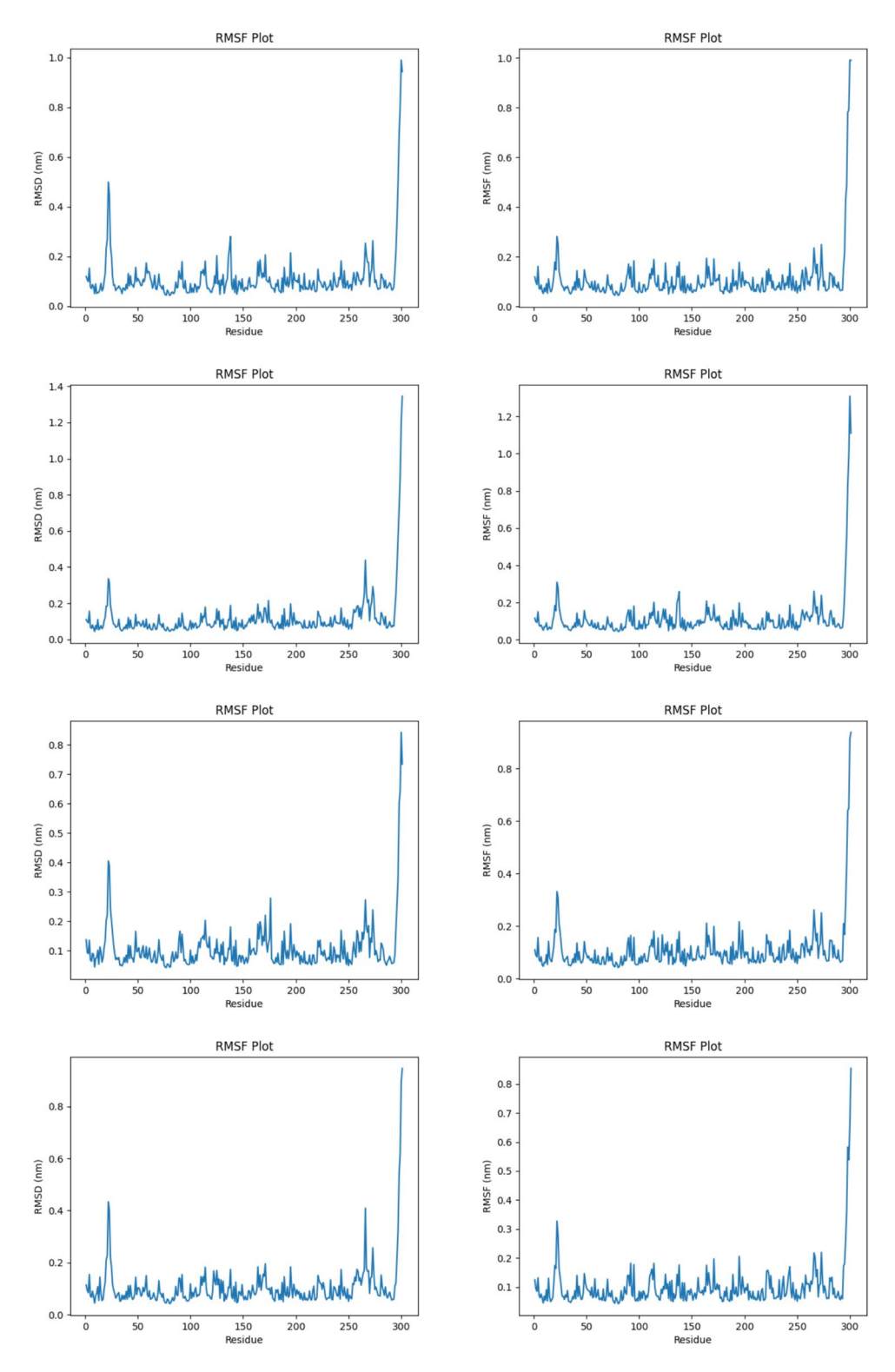
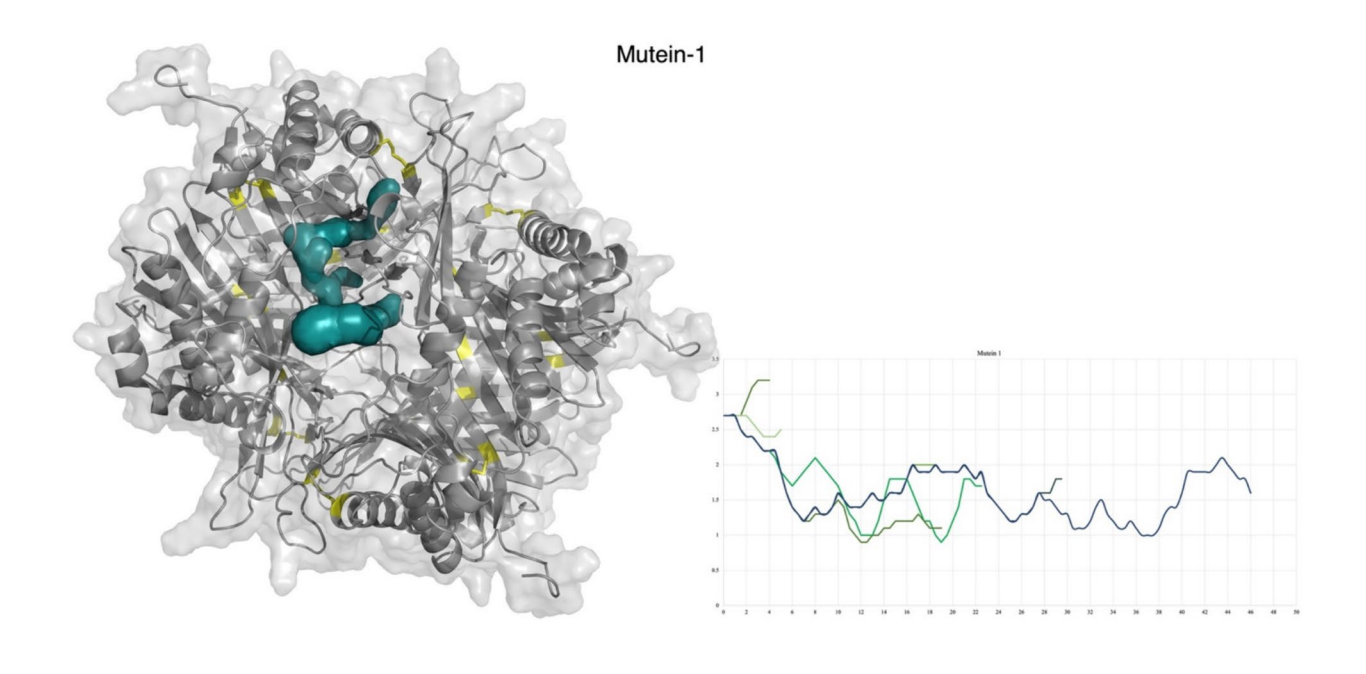


Fig. 8. RMSF profiles of wild-type A. flavus uricase (left panels) and disulfide-engineered mutein (right panels) across all residues. Each row represents one simulation replicate. Both variants display similar flexibility patterns with prominent peaks at residue \sim 25 and the C-terminus (residue \sim 301). The mutein maintains the essential dynamic properties of the wild-type enzyme while exhibiting subtle reductions in localized flexibility, demonstrating structural reinforcement without compromising functional motion.



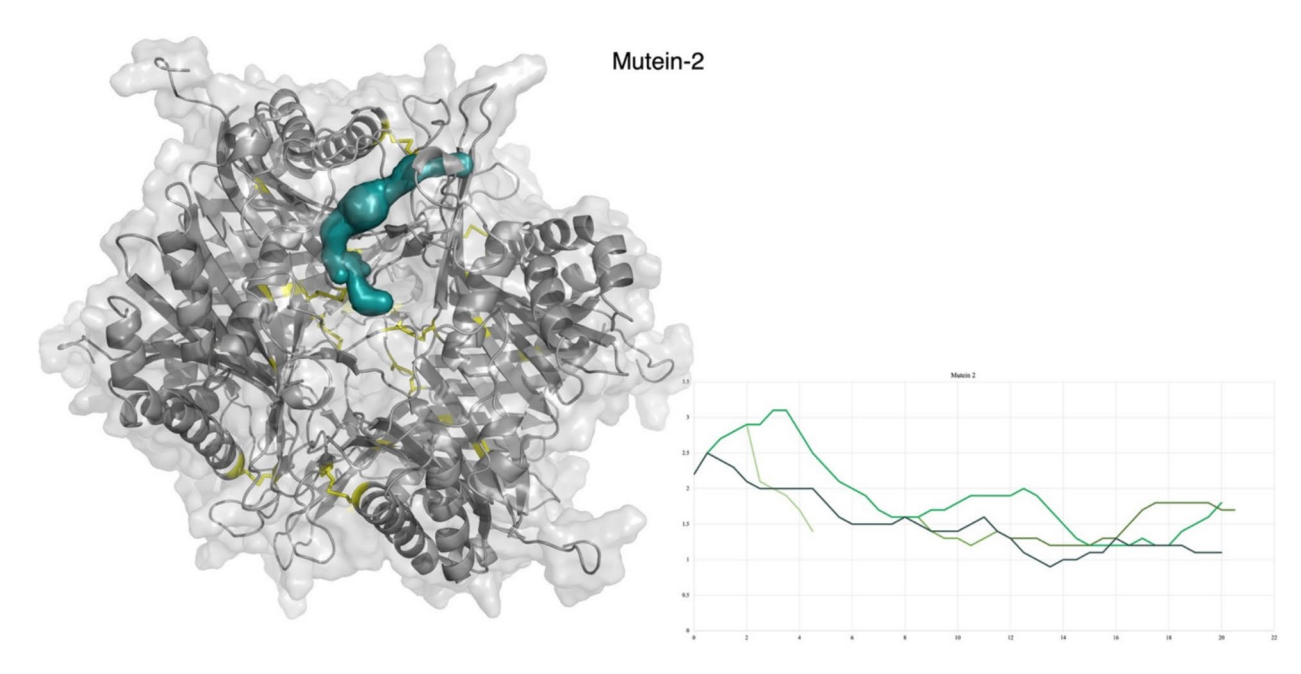
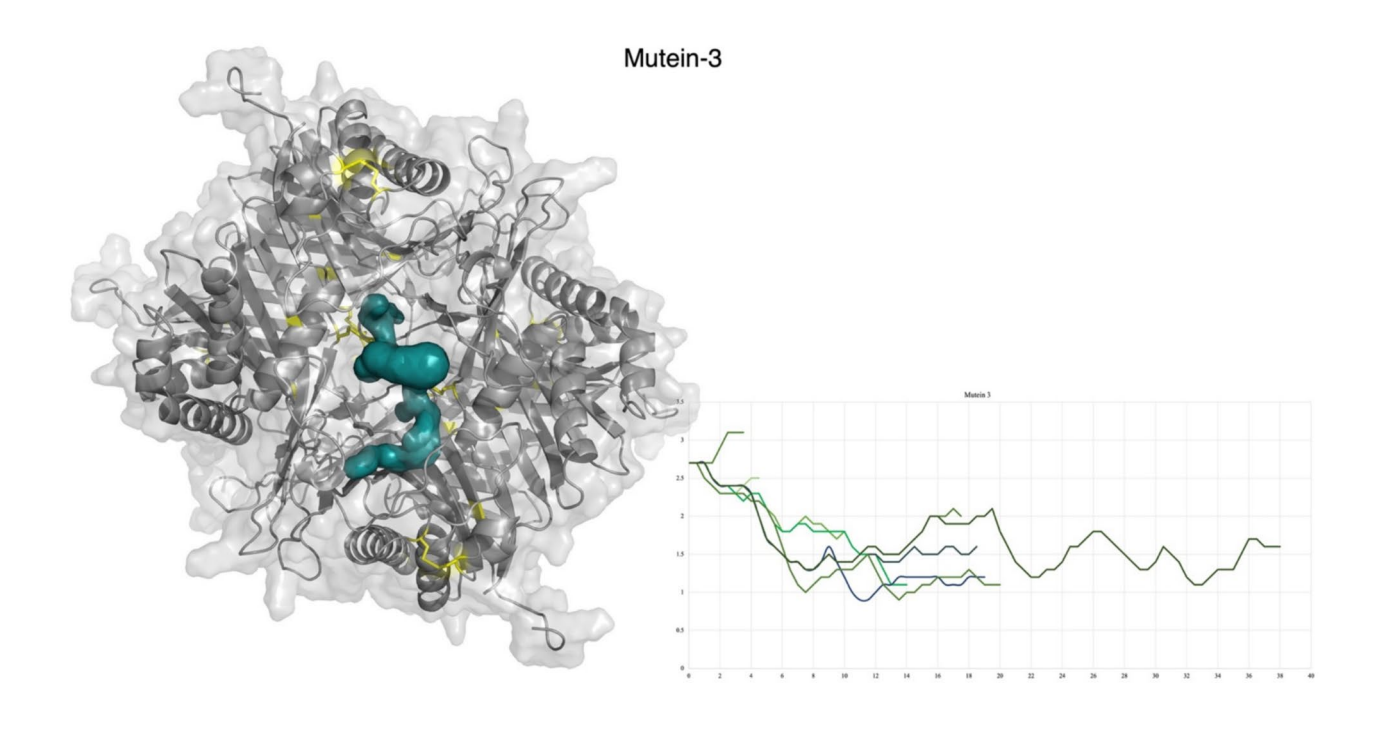


Fig. 9. Tunnel visualization and profile to the active site in uricase muteins. The tunnel profile provides insights into the potential accessibility of the active site and any potential bottlenecks or constrictions introduced by the mutations. The left panel shows the enzyme structure with a transparent surface representation. The backbone is rendered as gray cartoon ribbons, indicating secondary structures. Cysteine residues involved in disulfide bonding are highlighted in yellow, with corresponding bonds displayed as yellow sticks. The active site tunnel is visualized as a green surface. The right panel presents a profile of tunnel radii along their depths, with the x-axis representing tunnel depth and the y-axis the tunnel radius in Ångströms. The tunnel profile provides insights into the potential accessibility of the active site and any potential bottlenecks or constrictions introduced by the mutations. Image created using PyMOL version 3.0.0.

Muteins 1 to 6 generally show fewer total contacts and van der Waals interactions compared to the wild type, but an increase in hydrophobic interactions might counterbalance these losses, particularly in Mutein 3.

The absence of water-mediated hydrogen bonds and polar contacts might impact the overall flexibility and function of the muteins, though this doesn't necessarily imply a reduction in stability.

Muteins 3, 4, and 5, which showed high energetic stability based on previous total energy and frustration analyses, have a consistent pattern of maintaining hydrogen bonds and increasing hydrophobic contacts, reinforcing their potential as more stable variants.



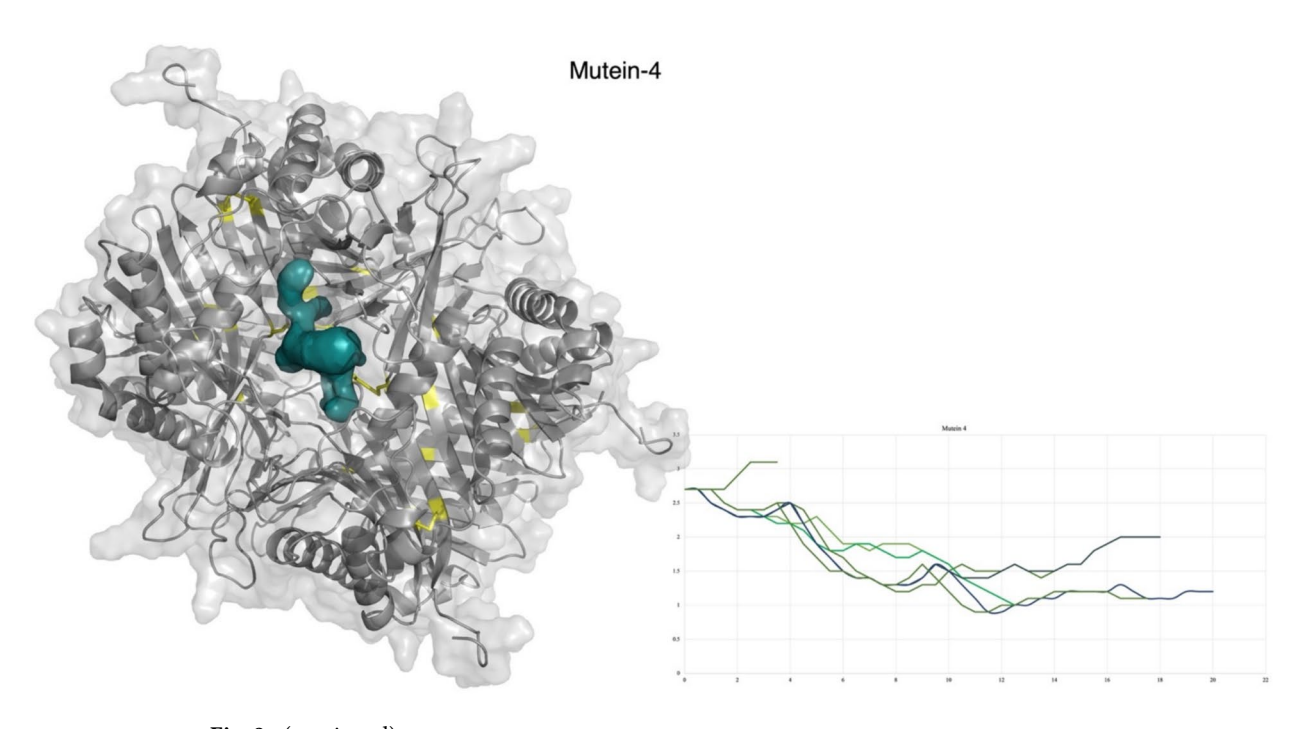
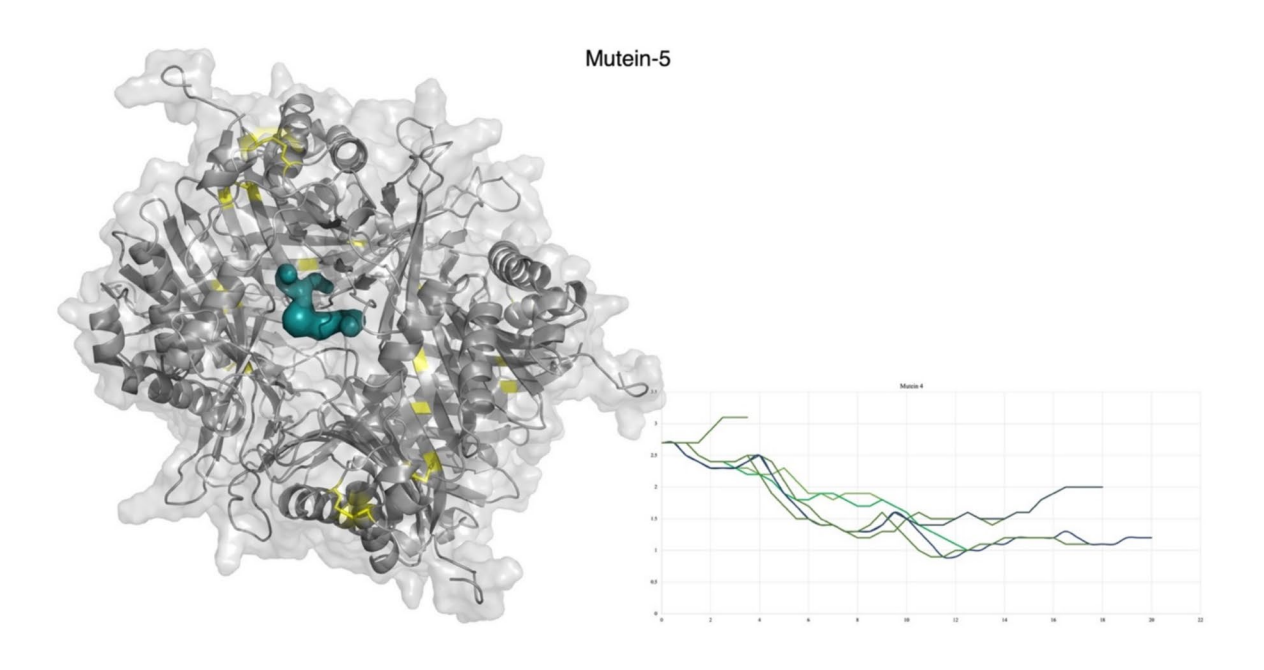


Fig. 9. (continued)

Discussion

This study aimed to enhance the stability of Aspergillus flavus uricase by introducing disulfide bonds at strategically selected positions, thereby reinforcing the enzyme's structural integrity and maintaining catalytic efficiency. Through in silico tools, eight positions were identified for disulfide bond formation, generating muteins with optimized stability profiles. The findings revealed that certain muteins exhibited significant reductions in energetic frustration and RMSF values, indicating enhanced stability. Additionally, tunnel profiling suggested that some muteins preserved or even improved substrate access to the active site, highlighting the potential for increased catalytic durability.



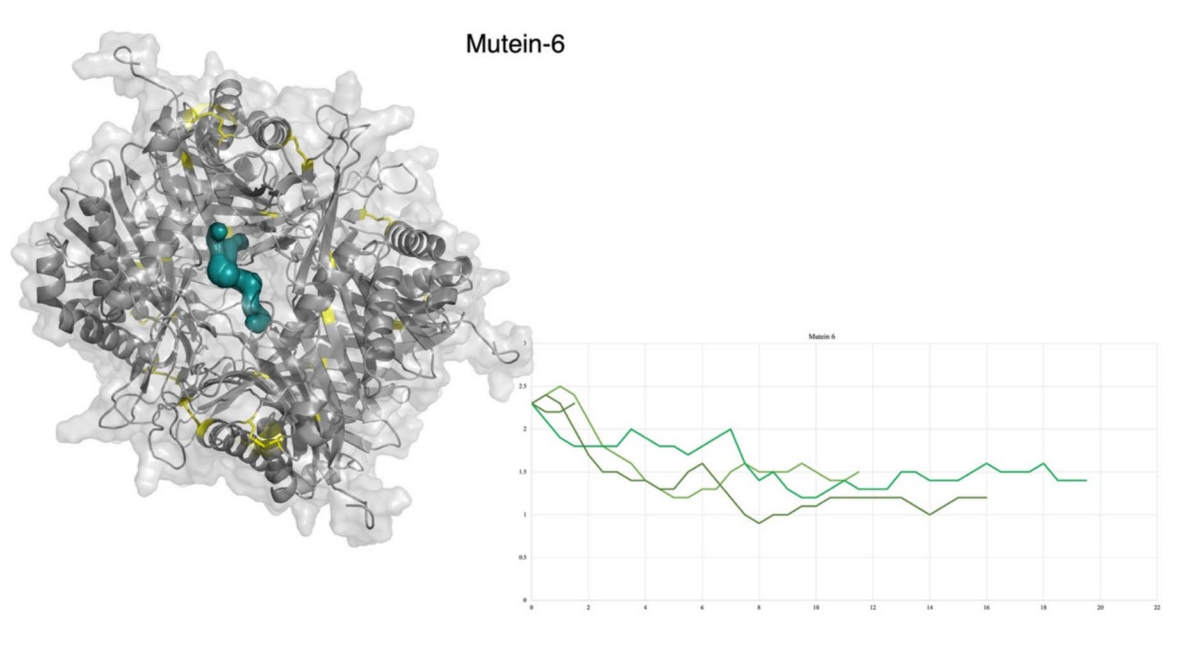


Fig. 9. (continued)

The introduction of disulfide bonds notably impacted the structural stability of uricase, as reflected in the energetic frustration and RMSF analyses. Muteins with disulfide bonds positioned away from the active site tunnel showed considerable decreases in highly frustrated density, suggesting a more stable overall fold. This effect aligns with prior research, such as Craig and Dombkowski's work (2013), which demonstrated that disulfide bonds could significantly reduce conformational entropy and enhance protein stability⁷.

The strategic introduction of disulfide bonds at the inter-subunit interfaces of the *A. flavus* uricase represents a rational approach to enhance therapeutic potential through improved structural stability. Our molecular

	WT	Mutein 1	Mutein 2	Mutein 3	Mutein 4	Mutein 5	Mutein 6
E-bound	-4	-4.2	-5.3	-4.1	-4.1	13.1	-6.3
E-max	-3.8	-4.1	-5.1	-3.8	-3.7	13.1	-4.5
E-surface	-4.7	-4.7	-5.6	-4.6	-4.6	-4.9	-4.5
Ea	0.9	0.6	0.5	0.8	0.9	18	0
ΔEBS	0.7	0.5	0.3	0.5	0.5	18	-1.8

Table 9. The energetic states of the tunnel to the active site of the enzyme. E-bound: Binding energy of the substrate within the tunnel. E-max: Maximum energy barrier along the tunnel pathway. E-surface: Energy at the tunnel entrance on the protein surface. Ea: Activation energy or energetic difference from the surface to the active site. ΔEbs (Energy Difference between Bound State and Surface): Energy difference between the substrate bound state and the unbound state.

dynamics analyses reveal that the engineered cysteine mutations successfully reinforce the quaternary structure without perturbing the enzyme's intrinsic flexibility profile. The preserved dynamic behavior, particularly in regions proximal to the active site, suggests retention of catalytic efficiency despite the enhanced structural rigidity. This engineered stability-function balance addresses a critical challenge in therapeutic enzyme development, potentially extending shelf-life and in vivo half-life while maintaining optimal catalytic parameters. The subtle reductions in RMSF values across multiple regions of the mutein further indicate a globally stabilized structure, likely contributing to enhanced resistance against thermal and chemical denaturation.

In our study, muteins like Mutein-1 and Mutein-3, which contained disulfide bonds at positions adjacent to structurally flexible regions, exhibited the most pronounced reductions in frustration density. This suggests that careful placement of disulfide bonds can stabilize the enzyme without imposing excess rigidity on the active regions.

Our results indicate that strategic disulfide bond placement can mitigate energetic frustrations, leading to enhanced stability. The addition of disulfide bonds in uricase muteins has reduced the presence of highly frustrated regions, which suggests that introducing covalent constraints helps in minimizing non-native interactions and stabilizes the overall fold. Sun et al. (2018) demonstrated the influence of nonnative energetic frustrations on the folding of β -sandwich proteins, showing that such frustrations impact transition state stability 31 . In a similar vein, uricase muteins with reduced energetic frustration potentially stabilize the transition state, making the enzyme fold more efficiently. This aligns with the observed decreases in frustration density for specific muteins, suggesting that disulfide bond formation may alleviate non-native interactions, a crucial factor in achieving a stable, functionally active state.

The role of frustration in modulating the dynamics of protein complexes, especially those involving intrinsically disordered regions was underscored previously³². In uricase muteins, the reduced frustration may also correspond to optimized conformational entropy in structurally flexible regions. By minimizing frustration, we may enhance the stability of regions that would otherwise exhibit disordered or highly dynamic behavior, contributing to a more predictable and stable fold under physiological conditions.

Tripathi et al. (2015) highlighted the role of charge interactions in alleviating frustration and enhancing thermal stability³³. Although disulfide bonds are covalent, the reduction in frustration observed in muteins suggests that they might also optimize electrostatic interactions by constraining the protein in a more favorable conformation. This constrained conformation could alleviate frustrations associated with exposed charged residues, thus facilitating a smoother and more efficient folding process that is energetically favorable.

Vilanova et al. (2014) found that ionic strength modulates energetic frustrations in protein structures, emphasizing how environmental factors contribute to protein stability. In the context of uricase muteins, disulfide bonds appear to stabilize regions that may otherwise be sensitive to ionic strength variations. This stability indicates that the modifications not only reduce intrinsic frustration but also buffer the enzyme against environmental fluctuations, which can be crucial for applications requiring consistent enzyme performance under varying conditions.

Evolutionary pressures shape frustration patterns in protein families³⁴. For uricase, an enzyme with therapeutic potential, evolutionary design principles may inherently favor stability-enhancing mutations. The observed reductions in local frustration patterns in your muteins may reflect an evolutionary-like optimization, suggesting that such modifications could align with the enzyme's natural folding and stability constraints.

It's important to note that the specific effects of disulfide bonds on uricase can vary depending on factors such as the source of the enzyme, the location of the disulfide bonds, and the overall protein structure.

Disulfide bonds can significantly improve the thermostability of *Arthrobacter globiformis* Uricase by preventing the disassociation of the multimeric enzyme assembly and stabilizing flexible loops in each subunit of the enzyme³⁵.

Studies have shown that introducing intersubunit cysteine pair mutations, like K12 C–E286 C, into Arthrobacter globiformis Uricase can create disulfide bonds that crosslink the subunits and prevent disassociation and unfolding³⁵. These mutations lead to increased unfolding temperatures and higher Δ Gdiss (Δ Gdiss indicates the free energy of tetramer or dimer dissociation in kcal/mol) values, indicating stronger dimer interfaces that are more difficult to dissociate.

In addition to enhanced thermostability, disulfide cross-linking can also protect uricase from protease digestion by fixing flexible loops and decreasing the surface area exposed to proteases2.

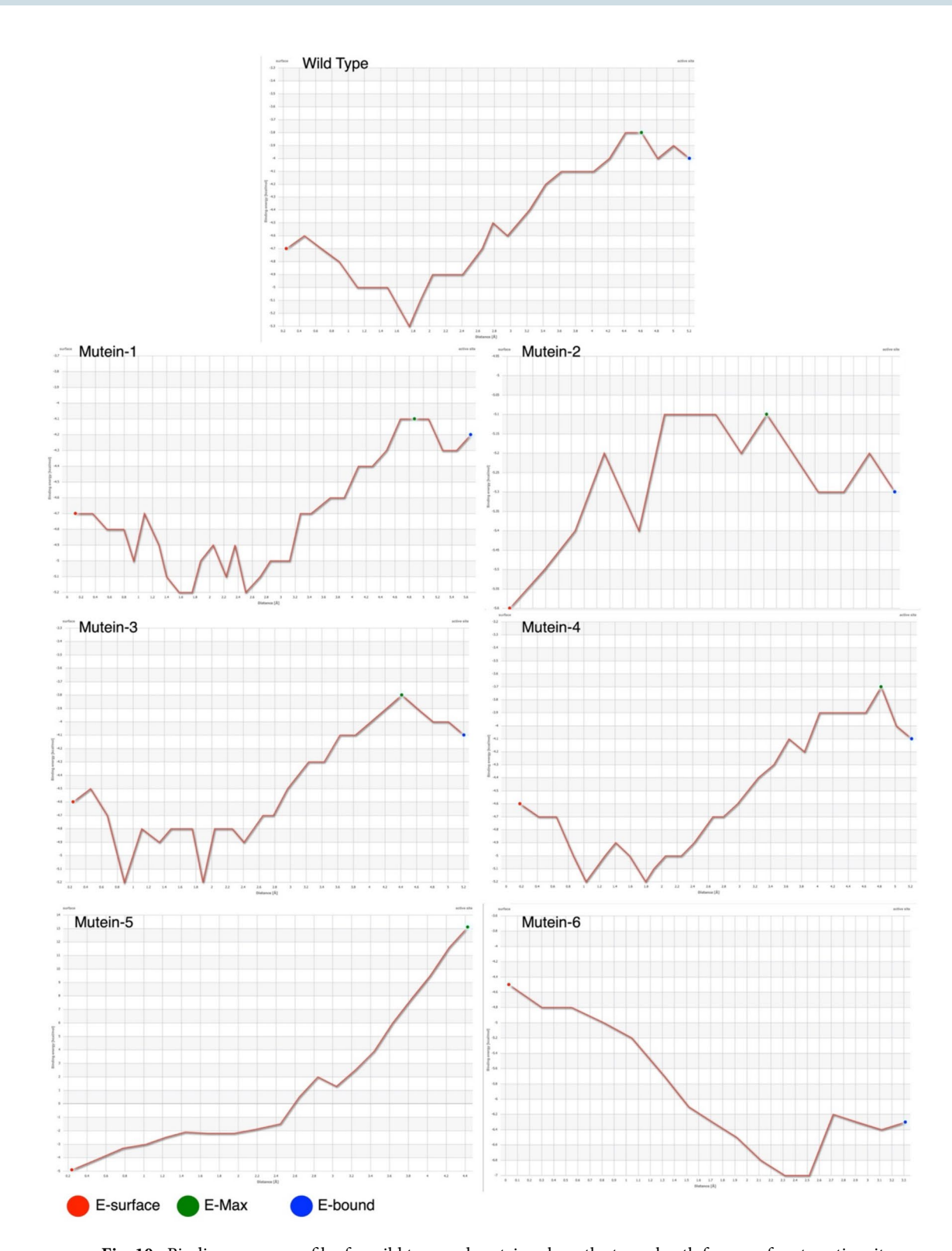


Fig. 10. Binding energy profiles for wild type and muteins along the tunnel path from surface to active site. This figure depicts the binding energy profiles of uric acid substrate as it traverses the tunnel leading to the active site in various uricase mutants. X-axis shows distance from surface to active site (Å), and Y-axis indicates binding energy (kcal/mol). Red, green, and blue dots represent surface binding energy, maximum binding energy, and active site binding energy, respectively. The red line represents the energy barrier for substrate transition through the tunnel.

	Total energy	Total diff to parent
Mutein 1	-2529.49	-336.86
Mutein 2	-2550.94	-315.41
Mutein 3	-2838.05	-28.3
Mutein 4	-2829.17	-37.18
Mutein 5	-2839.64	-26.71
Mutein 6	-2530.17	-336.18

Table 10. Total energy and difference to the wild type.

	Wild type	Mutein 1	Mutein 2	Mutein 3	Mutein 4	Mutein 5	Mutein 6
Mutually exclusive interactions				,			
Total number of contacts	24,312	9492	9397	9426	9491	9457	9444
VdW interactions	332	134	132	130	134	132	131
VdW clash interactions	2390	261	260	258	263	260	259
Covalent interactions	114	0	0	0	0	0	0
Covalent clash interactions	6	0	0	0	0	0	0
Proximal	21,470	9097	9005	9038	9094	9065	9054
Polar contacts				'			
Polar contacts	436	345	346	344	351	342	343
Water mediated polar contacts	2840	0	0	0	0	0	0
Weak polar contacts	212	246	246	240	245	242	244
Water mediated weak polar contacts	296	0	0	0	0	0	0
Feature contacts				•			
Hydrogen bonds	286	227	225	224	228	225	225
Water mediated hydrogen bonds	2554	0	0	0	0	0	0
Weak hydrogen bonds	192	197	196	192	195	192	195
Water mediated weak hydrogen bonds	310	0	0	0	0	0	0
Halogen bonds	0	0	0	0	0	0	0
Ionic interactions	32	34	34	34	34	34	34
Metal complex interactions	0	0	0	0	0	0	0
Aromatic contacts	12	16	16	16	16	16	16
Hydrophobic contacts	380	409	402	418	419	418	405
Carbonyl interactions	60	52		52	52	52	52

Table 11. Number of interactions and contacts.

The location of disulfide bonds can influence their effect on uricase. For instance, in *Gallus gallus* uricase, C287, C14*, and C289 are positioned near the "peroxo hole" and are thought to play a role in the reduction of 5-hydroxyisourate, possibly through solvent-mediated electron transfer¹.

While disulfide bonds generally stabilize protein structure, incorrect disulfide bonds can lead to protein aggregation or degradation. For example, heat treatment can cause the formation of interchain disulfide bonds in Candida uricase, leading to decreased activity².

While the study demonstrates the successful enhancement of stability in *Aspergillus flavus* uricase through the introduction of de novo disulfide bonds., the generalizability of this approach to other enzymes warrants careful consideration due to variations in protein structure, folding, and stability requirements^{2,36}. The successful application of disulfide engineering to other enzymes requires a structure-based approach, where the enzyme's tertiary structure analyzed to identify suitable locations for cysteine mutations that would form stabilizing disulfide bridges without disrupting the active site or overall protein conformation^{37,38}. The location of engineered disulfides can drastically affect protein stability, and some engineered disulfides may even decrease enzymatic activity^{8,39-41}. For instance, the introduction of a single disulfide bond in the distal region of manganese peroxidase (MnP) stabilized its heme environment, whereas the addition of a second engineered bond in the proximal region seemed to add a measure of instability1⁴⁰. Furthermore, the study of *Arthrobacter globiformis* uricase showed that specific mutations like K12 C–E286 C and S296 C–S296 C greatly increased thermostability, while others did not improve stability⁴¹. Therefore, the design of disulfide bonds needs to be tailored to each specific protein⁸. Computational tools like the Disulfide by Design 2.0 program can aid in predicting potential disulfide bridge locations by evaluating parameters like energy and χ3 values³⁷. Additionally, methods such as site-directed mutagenesis, SDS-PAGE, and thermal shift assays (TSA) are crucial for confirming the formation of the disulfide bonds and their impact on enzyme stability^{35,42,43}. Ultimately, while the principles of disulfide

bond engineering are generally applicable, the specific mutations and outcomes will be enzyme-dependent, necessitating thorough structural analysis and experimental validation for each target protein^{43,44}.

The effect of disulfide bonds on the compactness of uricase molecules has been studied through measurements of partial specific volume, adiabatic compressibility, and thermal expansibility during reduction. The findings suggest that reduction of disulfide bonds decreases internal cavities and increases surface hydration, indicating a decrease in compactness⁴⁵.

The number and location of disulfide bonds are important factors in determining their effects on uricase. Adiabatic compressibility values of native or oxidized proteins tend to decrease as the number of disulfide bonds increases, and these effects become more pronounced when disulfide bonds are formed over larger distances in the primary structure⁴⁵.

While disulfide bonds can stabilize the enzyme structure, they may also reduce flexibility in regions where molecular motion is critical for substrate binding, or for the release of the reaction products⁴⁶. The RMSF analysis highlighted this balance⁴⁷: Although the overall flexibility decreased in all muteins, certain positions maintained flexibility essential for catalysis. Notably, Mutein-3 and Mutein-1, which showed a significant decrease in frustration scores, also exhibited a significant reduction of RMSF values in the regions where mutations were introduced. This suggests an increase in local rigidity directly related to the disulfide bond and it shows that the mutations have a direct effect on the protein structure. However, since the overall activity of the enzyme was maintained, it is possible to infer that the overall flexibility of the active site was preserved, despite the local rigidity. As such, our results suggest a subtle balance between local rigidification and maintenance of overall enzymatic activity^{8,48}. Therefore, disulfide bond placement should consider local flexibility requirements alongside stability goals, as excessive rigidity could affect the enzyme's function and potentially limit catalytic turnover.

The tunnel profiling analysis indicated that certain muteins preserved or even enhanced substrate accessibility. Muteins Mutein-1, Mutein-2, and Mutein-6 exhibited tunnel profiles similar to the wild type, suggesting that substrate access to the active site remained largely unimpeded by the additional disulfide bonds. In contrast, Mutein-5 showed drastic alterations in tunnel volume and depth, likely due to disulfide bond-induced structural shifts near the tunnel entrance. Such changes can impede substrate movement and affect overall enzymatic efficiency⁴⁹. These observations are consistent with findings from studies on other enzymes, where disulfide bond placement influenced substrate tunnels and sometimes restricted substrate flow to the active site⁵⁰. These results highlight the importance of balancing the flexibility and rigidity for optimal activity. Our findings also highlight the importance of considering tunnel geometry when introducing structural modifications, as these alterations can have direct implications for catalytic activity.

Our analyses revealed that muteins with unimpeded tunnel profiles, particularly SS1 and SS6, exhibited favorable binding energies, implying smoother substrate passage through the tunnel. The energy profiles of these muteins suggested they could maintain catalytic activity while benefiting from enhanced structural stability. This observation aligns with recent research on enzyme engineering, which emphasizes the need for modifications that balance stability improvements with preserved catalytic access⁵¹. Therefore, the positioning of disulfide bonds in relation to active site tunnels is crucial for designing enzymes that have both enhanced stability and high activity, and it also highlights the challenges of achieving such balance. Regions distant from the tunnel are more likely to bolster stability without compromising enzyme function.

The results of this study have meaningful implications for the design of therapeutic enzymes and industrial biocatalysts. By targeting specific positions for disulfide bond formation, we demonstrate a pathway to create more stable uricase variants that may have longer half-lives and reduced immunogenicity. For therapeutic applications, enhancing uricase stability could minimize degradation, allowing for more sustained uric acid reduction in patients^{8,35}. In industrial contexts, enzymes with increased stability are advantageous for processes requiring prolonged operation under variable or harsh conditions⁵². This study also suggests that disulfide bond engineering can be a valuable tool in enzyme design, as it offers a relatively straightforward approach to stability enhancement without extensive alterations to the enzyme's native structure.

Our approach to disulfide bond engineering distinguishes itself from other methods, such as directed evolution or chemical modifications, by strategically leveraging covalent linkages to stabilize specific regions. While directed evolution can yield enzymes with optimized catalytic properties, it often requires extensive rounds of selection and screening. In contrast, targeted disulfide bond introduction enables more predictable outcomes, particularly when combined with computational tools for frustration and tunnel profiling. This integration of structural and functional analyses provides a powerful framework for designing enzymes that not only maintain, but also enhance, their operational stability and activity.

While this study offers insights into the stabilization of uricase through disulfide bond engineering, it is essential to recognize its limitations. The predictions and analyses are based on in silico modeling, and experimental validation is needed to confirm the stability and activity profiles observed in the simulations. Additionally, the rigidity introduced by disulfide bonds may have unforeseen impacts on catalytic efficiency in physiological environments, an aspect that in vivo studies could clarify. Future research could involve expressing these muteins in a host system and performing kinetic assays to evaluate their stability and catalytic efficiency under therapeutic conditions.

Protein expression and purification is the first step in validating the computational predictions. The mutant uricase genes would need to be cloned and expressed in a suitable host organism, such as *E. coli*. Following expression, the recombinant proteins would be purified to homogeneity using methods like Ni–NTA chromatography and gel filtration¹. The purity of the proteins would be confirmed through SDS-PAGE analysis².

The enzymatic activity of the purified mutant uricases must be determined by measuring their ability to convert uric acid to allantoin³⁷. This would include establishing kinetic parameters such as Km and kcat, which help assess the catalytic efficiency of the enzymes. In the case of the study of Latimeria menadoensis uricase,

it was reported that the catalytic efficiency (kcat/Km) of some of the mutants was lower than the wild type³⁷. Therefore, it is important to confirm the activity is not compromised by the mutation.

To ensure that the designed disulfide bonds have formed correctly, methods such as thiol titration with Ellman's reagent should be used⁸. This technique helps determine the number of free thiol groups, where a decrease in free thiols can indicate disulfide bond formation.

The thermostability of the mutant enzymes would be assessed using techniques such as differential scanning fluorimetry. A shift in melting temperature (Tm) would indicate enhanced stability due to the introduced disulfide bonds⁴¹. The thermal stability can be further assessed by measuring residual activity after incubation at elevated temperatures. Furthermore, the use of circular dichroism (CD) spectroscopy can confirm the secondary structure of the protein and monitor its stability at different temperatures³⁷.

Further investigations could explore the applicability of this disulfide bond engineering strategy to other enzymes with similar structural characteristics. Extending the analysis to other enzymes with complex quaternary structures and active site tunnels could provide valuable insights into the generalizability of these findings. Additionally, conducting in vivo studies could shed light on how these modified enzymes perform under physiological conditions, offering a clearer picture of their therapeutic potential.

Conclusion

This study demonstrates the effectiveness of disulfide bond engineering in enhancing uricase stability, offering a promising pathway for improving enzyme performance in challenging environments. By strategically introducing disulfide bonds, we achieved significant reductions in structural frustration and local flexibility, translating into increased stability across several muteins. The integrated analysis of frustration density, RMSF, and tunnel accessibility provides a holistic view of how structural modifications impact both stability and catalytic efficiency. Muteins 1 and 3 emerged as particularly promising candidates, exhibiting a balanced profile of enhanced stability and maintained substrate accessibility. These findings underline the importance of selecting optimal disulfide sites to preserve enzymatic function while achieving structural resilience. This approach paves the way for the development of robust biocatalysts that can meet the demands of therapeutic applications and industrial processes.

Data availability

All data generated or analysed during this study are included in this paper, its supplementary material, and in publicly available repositories including Uniprot Knowledge Base at www.uniprot.org, Protein Data Bank at www.rcsb.org, and PubChem https://pubchem.ncbi.nlm.nih.gov/.

Received: 21 October 2024; Accepted: 7 May 2025

Published online: 26 May 2025

References

- Mori, G. et al. Cysteine enrichment mediates co-option of uricase in reptilian skin and transition to uricotelism. Mol. Biol. Evol. 40(9), msad200 (2023).
- 2. Tao, L. et al. Designing a mutant Candida uricase with improved polymerization state and enzymatic activity. *Protein Eng. Des. Sel.* **30**(11), 753–759 (2017).
- 3. Chiu, Y.-C., Hsu, T.-S., Huang, C.-Y. & Hsu, C.-H. Structural and biochemical insights into a hyperthermostable urate oxidase from thermobispora bispora for hyperuricemia and gout therapy. *Int. J. Biol. Macromol.* **188**, 914–923 (2021).
- Keebaugh, A. C. & Thomas, J. W. The evolutionary fate of the genes encoding the purine catabolic enzymes in hominoids, birds, and reptiles. Mol. Biol. Evol. 27(6), 1359–1369 (2010).
- 5. Garay, R. P., El-Gewely, M. R., Labaune, J.-P. & Richette, P. Therapeutic perspectives on uricases for gout. *Joint Bone Spine* 79(3), 237–242 (2012).
- 19(10), 640–649 (2023). Exercise F. & Lioté, F. Mechanisms and rationale for uricase use in patients with gout. *Nat. Rev. Rheumatol.* 19(10), 640–649 (2023).
- 7. Colloc'h, N. et al. Crystal structure of the protein drug urate oxidase-inhibitor complex at 2.05 Å resolution. *Nat. Struct. Biol.* 4(11), 947–952 (1997).
- Retailleau, P. et al. Complexed and ligand-free high-resolution structures of urate oxidase (Uox) from Aspergillus flavus: A reassignment of the active-site binding mode. Acta. Crystallogr. Sect. D: Biol. Crystallogr. 60(3), 453–462 (2004).
- 9. Chen, X.-y et al. The effect of hyperuricemia and its interaction with hypertension towards chronic kidney disease in patients with type 2 diabetes: evidence from a cross-sectional study in Eastern China. *Front. Endocrinol. (Lausanne)* https://doi.org/10.3389/fendo.2024.1415459 (2024) (Original research).
- Craig, D. B. & Dombkowski, A. A. Disulfide by design 2.0: A web-based tool for disulfide engineering in proteins. BMC Bioinform. 14, 1–7 (2013).
- 11. Marjani, L. R., Imani, M. & Jaliani, H. Z. Enhancement of pharmaceutical urate oxidase thermostability by rational design of de novo disulfide bridge. *Iran. J. Biotechnol.* **18**(3), e2662 (2020).
- 12. Tsai, C.-H. et al. Bioinformatics approaches for disulfide connectivity prediction. Curr. Protein Pept. Sci. 8(3), 243-260 (2007).
- Zhou, L. et al. Unlocking the potential of enzyme engineering via rational computational design strategies. Biotechnol. Adv. 73, 108376. https://doi.org/10.1016/j.biotechadv.2024.108376 (2024).
- 14. Jurich, C.; Śhao, Q.; Ran, X.; Yang, Z. Physics-based Modeling in the New Era of Enzyme Engineering Son, A.; Park, J.; Kim, W.; Yoon, Y.; Lee, S.; Park, Y.; Kim, H. Revolutionizing molecular design for innovative therapeutic applications through artificial intelligence. *Molecules* 2024 29 (19) 4626
- 15. Wang, X., Xu, K., Zeng, X., Linghu, K., Zhao, B., Yu, S., Wang, K., Yu, S., Zhao, X., Zeng, W. et al. Machine learning-assisted substrate binding pocket engineering based on structural information. *Brief. Bioinform.* https://doi.org/10.1093/bib/bbae381 Accessed 1 26 2025 (2024).
- Burley, S. K. et al. RCSB Protein data bank (RCSB.org): Delivery of experimentally-determined PDB structures alongside one million computed structure models of proteins from artificial intelligence/machine learning. *Nucl. Acid. Res.* 51, D488–D508 (2022).
- 17. Bateman, A. et al. UniProt: the universal protein knowledgebase in 2021. Nucl. Acid. Res. 49, D480-D489 (2020).

- 18. Laimer, J., Hiebl-Flach, J., Lengauer, D. & Lackner, P. MAESTROweb: A web server for structure-based protein stability prediction. *Bioinformatics* 32(9), 1414–1416 (2016).
- 19. Leman, J. K. et al. Macromolecular modeling and design in Rosetta: Recent methods and frameworks. Nat. Method. 17(7), 665–680 (2020).
- 20. Eddy, S. R. Profile hidden Markov models. Bioinformatics (Oxford, England) 14(9), 755-763 (1998).
- 21. Smith, T. F. & Waterman, M. S. Identification of common molecular subsequences. J. Mol. Biol. 147(1), 195-197 (1981).
- 22. Suplatov, D. A., Kopylov, K. E., Popova, N. N., Voevodin, V. V. & Švedas, V. K. Mustguseal: A server for multiple structure-guided sequence alignment of protein families. *Bioinformatics* 34(9), 1583–1585 (2018).
- 23. Rodrigues, C. H., Pires, D. E. & Ascher, D. B. DynaMut2: Assessing changes in stability and flexibility upon single and multiple point missense mutations. *Protein Sci.* **30**(1), 60–69 (2021).
- 24. Philipp, M., Moth, C. W., Ristic, N., Tiemann, J. K. S., Seufert, F., Panfilova, A., Meiler, J., Hildebrand, P. W., Stein, A., Wiegreffe, D. MutationExplorer: A webserver for mutation of proteins and 3D visualization of energetic impacts *Nucl. Acid. Res.* gkae301 (2024).
- McGuffin, L. J., Edmunds, N. S., Genc, A. G., Alharbi, S. M. A., Salehe, Bajuna R., Adiyaman, R. Prediction of protein structures, functions and interactions using the IntFOLD7, MultiFOLD and ModFOLDdock servers. *Nucl. Acid. Res.* 51 (W1), W274-W280. https://doi.org/10.1093/nar/gkad297 Accessed 10/13/2024 (2023).
- Adiyaman, R.; Edmunds, N. S.; Genc, A. G.; Alharbi, S. M. A.; McGuffin, L. J. Improvement of protein tertiary and quaternary structure predictions using the ReFOLD refinement method and the AlphaFold2 recycling process. *Bioinform. Adv.* 3(1) https://doi.org/10.1093/bioadv/vbad078 Accessed 10/13/2024 (2023).
- 27. Shapovalov, M. V. & Dunbrack, R. L. Jr. A smoothed backbone-dependent rotamer library for proteins derived from adaptive kernel density estimates and regressions. *Structure* 19(6), 844–858 (2011).
- 28. Parra, R. G. et al. Protein Frustratometer 2: A tool to localize energetic frustration in protein molecules, now with electrostatics. *Nucl. Acid. Res.* 44(W1), W356–W360 (2016).
- 29. Kuriata, A. et al. CABS-flex 2.0: A web server for fast simulations of flexibility of protein structures. *Nucl. Acid. Res.* 46(W1), W338–W343 (2018).
- 30. Abraham, M. J. et al. GROMACS: High performance molecular simulations through multi-level parallelism from laptops to supercomputers. *SoftwareX* 1, 19–25 (2015).
- 31. Christen, M. et al. The GROMOS software for biomolecular simulation: GROMOS05. J. Comput. Chem. 26(16), 1719–1751 (2005).
- 32. Stourac, J. et al. Caver Web 1.0: Identification of tunnels and channels in proteins and analysis of ligand transport. *Nucl. Acid. Res.* 47(W1), W414–W422 (2019).
- 33. Jubb, H. C. et al. Arpeggio: A web server for calculating and visualising interatomic interactions in protein structures. *J. Mol. Biol.* **429**(3), 365–371 (2017).
- 34. Waterhouse, A. M., Procter, J. B., Martin, D. M., Clamp, M. & Barton, G. J. Jalview Version 2—a multiple sequence alignment editor and analysis workbench. *Bioinformatics* 25(9), 1189–1191 (2009).
- 35. Sun, Y., Ding, F. & Ming, D. Nonnative energetic frustrations in protein folding at residual level: A simulation study of homologous immunoglobulin-like β-sandwich proteins. *Int. J. Mol. Sci.* **19**(5), 1515 (2018).
- Lindstrom, I. & Dogan, J. Dynamics, conformational entropy, and frustration in protein-protein interactions involving an intrinsically disordered protein domain. ACS Chem. Biol. 13(5), 1218–1227 (2018).
- 37. Tripathi, S., Garcia, A. É. & Makhatadze, G. I. Alterations of nonconserved residues affect protein stability and folding dynamics through charge-charge interactions. *J. Phys. Chem. B* 119(41), 13103–13112 (2015).
- 38. Freiberger, M. I. et al. Local energetic frustration conservation in protein families and superfamilies. *Nat. Commun.* 14(1), 8379 (2023)
- 39. Shi, Y. et al. Structure-based design of a hyperthermostable AgUricase for hyperuricemia and gout therapy. *Acta Pharmacol. Sin.* **40**(10), 1364–1372 (2019).
- 40. Thornton, J. Disulphide bridges in globular proteins. J. Mol. Biol. 151(2), 261–287 (1981).
- 41. Azimi, I., Wong, J. W. & Hogg, P. J. Control of mature protein function by allosteric disulfide bonds. *Antioxid. Redox Signal.* 14(1), 113–126 (2011).
- 42. Takagi, H. et al. Enhancement of the thermostability of subtilisin E by introduction of a disulfide bond engineered on the basis of structural comparison with a thermophilic serine protease. J. Biol. Chem. 265(12), 6874–6878 (1990).
- 43. Villafranca, J. E., Howell, E. E., Oatley, S. J., Xuong, N. H. & Kraut, J. An engineered disulfide bond in dihydrofolate reductase. *Biochemistry* 26(8), 2182–2189 (1987).
- 44. Yainoy, S. et al. Production and characterization of recombinant wild type uricase from indonesian coelacanth (L. menadoensis) and improvement of its thermostability by in silico rational design and disulphide bridges engineering. *Int. J. Mol. Sci.* 20(6), 1269 (2019)
- 45. Eijsink, V. G. et al. Rational engineering of enzyme stability. J. Biotechnol. 113(1-3), 105-120 (2004).
- 46. Imani, M., Hosseinkhani, S., Ahmadian, S. & Nazari, M. Design and introduction of a disulfide bridge in firefly luciferase: Increase of thermostability and decrease of pH sensitivity. *Photochem. Photobiol. Sci.* **9**(8), 1167–1177 (2010).
- 47. Nyborg, A. C. et al. A therapeutic uricase with reduced immunogenicity risk and improved development properties. *PLoS ONE* 11(12), e0167935. https://doi.org/10.1371/journal.pone.0167935 (2016).
- 48. Reading, N. S. & Aust, S. D. Role of disulfide bonds in the stability of recombinant manganese peroxidase. *Biochemistry* **40**(27), 8161–8168 (2001).
- Bayol, A., Dupin, P., Boe, J., Claudy, P. & Létoffé, J. Study of pH and temperature-induced transitions in urate oxidase (Uox-EC1. 7.3. 3) by microcalorimetry (DSC), size exclusion chromatography (SEC) and enzymatic activity experiments. *Biophys. Chem.* 54(3), 229–235 (1995).
- 50. Pikal-Cleland, K. A., Rodríguez-Hornedo, N., Amidon, G. L. & Carpenter, J. F. Protein denaturation during freezing and thawing in phosphate buffer systems: Monomeric and tetrameric β-galactosidase. *Arch. Biochem. Biophys.* **384**(2), 398–406 (2000).
- 51. Jo, B. H. et al. Engineering de novo disulfide bond in bacterial α-type carbonic anhydrase for thermostable carbon sequestration. *Sci. Rep.* **6**(1), 29322 (2016).
- 52. Sugimoto, H. et al. Thermodynamic effects of disulfide bond on thermal unfolding of the starch-binding domain of Aspergillus niger glucoamylase. *Biosci. Biotechnol. Biochem.* 71(6), 1535–1541 (2007).

Author contributions

All authors contributed to the study's conception and design. M.R.R., N.N., and M.H.M. wrote the first draft of the manuscript. The final edition was edited and approved by Y.Gh., M.B.Gh.. A.S. significantly contributed to the data analysis and statistical analysis. M.S.H. performed the Molecular dynamics simulations, interpreted the results, generated the RMSD and RMSF graphs. All authors commented on previous versions of the manuscript. All authors read and approved the final manuscript.

Funding

The authors wish to thank Shiraz University of Medical Sciences (grant number: 15870) for supporting the conduct of this research.

Declarations

Competing interests

The authors declare no competing interests.

Consent for publication

The authors affirm that provided informed consent for publication.

Additional information

Supplementary Information The online version contains supplementary material available at https://doi.org/1 0.1038/s41598-025-01683-y.

Correspondence and requests for materials should be addressed to Y.G.

Reprints and permissions information is available at www.nature.com/reprints.

Publisher's note Springer Nature remains neutral with regard to jurisdictional claims in published maps and institutional affiliations.

Open Access This article is licensed under a Creative Commons Attribution-NonCommercial-NoDerivatives 4.0 International License, which permits any non-commercial use, sharing, distribution and reproduction in any medium or format, as long as you give appropriate credit to the original author(s) and the source, provide a link to the Creative Commons licence, and indicate if you modified the licensed material. You do not have permission under this licence to share adapted material derived from this article or parts of it. The images or other third party material in this article are included in the article's Creative Commons licence, unless indicated otherwise in a credit line to the material. If material is not included in the article's Creative Commons licence and your intended use is not permitted by statutory regulation or exceeds the permitted use, you will need to obtain permission directly from the copyright holder. To view a copy of this licence, visit http://creativecommons.org/licenses/by-nc-nd/4.0/.

© The Author(s) 2025